

Speed-of-Sound Measurements and a Fundamental Equation of State for Propylene Glycol

Cite as: J. Phys. Chem. Ref. Data **50**, 023105 (2021); <https://doi.org/10.1063/5.0050021>
Submitted: 11 March 2021 • Accepted: 11 May 2021 • Published Online: 09 June 2021

 Tim Eisenbach, Christian Scholz,  Roland Span, et al.



View Online



Export Citation



CrossMark

ARTICLES YOU MAY BE INTERESTED IN

[New Equations of State for Binary Hydrogen Mixtures Containing Methane, Nitrogen, Carbon Monoxide, and Carbon Dioxide](#)

Journal of Physical and Chemical Reference Data **50**, 013102 (2021); <https://doi.org/10.1063/5.0040533>

[Equations of State for the Thermodynamic Properties of Binary Mixtures for Helium-4, Neon, and Argon](#)

Journal of Physical and Chemical Reference Data **49**, 023101 (2020); <https://doi.org/10.1063/1.5142275>

[Equations of State for the Thermodynamic Properties of Three Hexane Isomers: 3-Methylpentane, 2,2-Dimethylbutane, and 2,3-Dimethylbutane](#)

Journal of Physical and Chemical Reference Data **50**, 033103 (2021); <https://doi.org/10.1063/1.5093644>

Journal of Physical and
Chemical Reference Data

READ TODAY!

CODATA Recommended Values of the
Fundamental Physical Constants: 2018



Speed-of-Sound Measurements and a Fundamental Equation of State for Propylene Glycol

Cite as: J. Phys. Chem. Ref. Data 50, 023105 (2021); doi: 10.1063/5.0050021

Submitted: 11 March 2021 • Accepted: 11 May 2021 •

Published Online: 9 June 2021



View Online



Export Citation



CrossMark

Tim Eisenbach,^{1,a)} Christian Scholz,¹ Roland Span,¹ Diego Cristancho,² Eric W. Lemmon,³ and Monika Thol¹

AFFILIATIONS

¹Ruhr-Universität Bochum, Thermodynamics, 44801 Bochum, Germany

²Dow, Lake Jackson, Texas 77566, USA

³Applied Chemicals and Materials Division, National Institute of Standards and Technology, Boulder, Colorado 80305, USA

^{a)} Author to whom correspondence should be addressed: t.eisenbach@thermo.ruhr-uni-bochum.de

ABSTRACT

A fundamental equation of state was developed for propylene glycol. It is written in terms of the Helmholtz energy with the independent variables temperature and density. Due to its fundamental nature, it can be used to calculate all thermodynamic state properties from the Helmholtz energy and its derivatives with respect to the independent variables. Special attention was paid not only to accurately reproduce the available experimental data but also to correct extrapolation. Therefore, this equation can be used for application in mixture models. For the development of the present equation of state, the available literature data were supplemented with new experimental speed-of-sound measurements, which were conducted in the temperature range from 293.2 K to 353.2 K with pressures up to 20 MPa. High accuracy was achieved by applying the well-established double-path-length pulse-echo technique and a careful sample preparation.

© 2021 by the U.S. Secretary of Commerce on behalf of the United States. All rights reserved. <https://doi.org/10.1063/5.0050021>

Key words: equation of state; experimental measurements; extrapolation; Helmholtz energy; propylene glycol; speed of sound.

CONTENTS

1. Introduction	2	9. Comparison with Literature Data and Validation of the Equation of State	12
2. Characteristics of Propylene Glycol	3	9.1. Comparisons of homogeneous density data	13
3. Speed-of-Sound Measurements	3	9.2. Comparisons of vapor–liquid equilibrium data	15
3.1. Apparatus description	3	9.3. Comparisons of caloric properties	17
3.2. Calibration	4	10. Extrapolation and Physical Behavior	21
3.3. Measurement fluid	4	11. Conclusion	23
3.4. Experimental procedures	5	12. Supplementary Material	24
3.5. Results	5	Acknowledgment	24
4. Equation of State	6	Data Availability	24
4.1. Ideal contribution	6	13. References	24
4.2. Residual part	8		
5. Fitting Procedure	8		
6. Critical Point Determination	9		
7. Isobaric Heat Capacity of the Ideal Gas	10		
8. Equation of State for Propylene Glycol	11		

List of Tables

1. Molar mass and characteristic thermodynamic properties of propylene glycol and the universal gas constant	4
2. Sample information of the used experimental materials	5

3.	Speed-of-sound measurements in propylene glycol carried out with the pulse-echo sensor	6	density ρ' , and the saturated vapor density ρ'' from the equation of state	13
4.	Uncertainty budget for the speed-of-sound measurements in propylene glycol	6	5. p,T -diagram with all available data in relation to the vapor-pressure curve and the critical point	13
5.	Overview of all experimentally obtained and estimated critical properties of propylene glycol	9	6. Deviations of homogeneous liquid density data from the equation of state for selected datasets in selected temperature ranges as a function of the logarithmic pressure	15
6.	Parameters of the Planck–Einstein terms of the ideal part of the equation of state according to Eq. (17)	11	7. Deviations of homogeneous liquid density data of Bridgman from the equation of state as a function of the logarithmic pressure	15
7.	Parameters of the residual part of the equation of state for propylene glycol according to Eq. (18)	11	8. Deviations of homogeneous liquid density data from the equation of state at atmospheric pressure as a function of temperature	16
8.	Test values for the verification of computer implementation	12	9. Deviations of all available vapor-pressure data from the equation of state as a function of temperature	18
9.	Parameters of the ancillary equations for the vapor pressure p_v , the saturated liquid density ρ' , and the saturated vapor density ρ'' according to Eqs. (19)–(21)	12	10. Deviations of the available speed-of-sound data in the liquid phase from the equation of state in selected temperature ranges as a function of the logarithmic pressure along with the speed-of-sound data measured in this work	20
10.	Summary of all underlying experimental and estimated data points	13	11. Deviations of the available speed-of-sound data in the liquid phase from the equation of state at atmospheric pressure as a function of temperature	21
11.	Summary of available homogeneous liquid density data along with the temperature and pressure ranges and their overall AADs with respect to the equation of state	14	12. Deviations of all available liquid-phase isobaric-heat-capacity data from the equation of state as a function of temperature	21
12.	Summary of vapor–pressure (p_v) and saturated liquid density (ρ') data along with the temperature ranges and their AADs with respect to the equation of state	17	13. Ideal curves for the equation of state for propylene glycol (PGC) in terms of the reduced temperature T/T_c and pressure p/p_c :	22
13.	Summary of all liquid-phase speed-of-sound data along with the temperature and pressure ranges and their AADs with respect to the equation of state	19	14. p,ρ -diagram along isotherms up to 10^6 K (top). T,ρ -diagram showing the phase boundaries, the rectilinear diameter, and the critical isobar (bottom)	22
14.	Summary of all isobaric-heat-capacity data along with the temperature range and their overall AADs with respect to the equation of state	19	15. Second (B), third (C), and fourth (D) virial coefficients	22
List of Figures			16. Speed of sound along isobars up to 120 MPa as a function of temperature	23
1.	Results of the calibration speed-of-sound measurements in pure water	4	17. Residual isochoric heat capacity along isobars up to 50 MPa as a function of temperature	23
2.	Speed-of-sound measurements in propylene glycol as a function of pressure along four isotherms	5	18. Phase identification parameter as a function of temperature along selected isobars	23
3.	Deviations of the calculated ideal-gas isobaric-heat-capacity data from the equation of state	10	19. Residual Grüneisen parameter as a function of temperature along selected isobars	23
4.	Deviations of the values calculated with the ancillary equations for the vapor pressure p_v , the saturated liquid			

1. Introduction

In consideration of today's climate issues, optimization of facilities in process engineering and power generation becomes more and more important, in particular, the highly accurate investigation and understanding of the utilized fluids in process applications. Even though there is a vast quantity of fluids with a comprehensive data basis, in some fluid states (e.g., at high pressures and temperatures), experimental data with reasonable uncertainties are not easy to obtain with conventional measurements. To maintain access to highly precise fluid properties over a broad range of fluid states, equations of state can be developed to provide reference thermodynamic properties, which is also of major importance for fluids with a less comprehensive data basis.

This work provides an equation of state for propylene glycol, which represents the available literature data with an accuracy that is in line with

future requirements in mixture modeling. Propylene glycol is often used to lower the freezing point of water, e.g., when being applied as de-icing fluids for aircraft. Furthermore, it is frequently employed as a substitute for ethylene glycol in mixtures used in refrigerant processes because it is less toxic.¹ A somewhat more specific application of propylene glycol is its use as an inhibitor of gas hydrate formation. The effect of hydrate formation poses a high safety but also economic risk when drilling holes, e.g., for the use of offshore and deep-water reservoirs in the context of carbon capture and storage.²

In the course of the development of thermodynamic models for CO₂-rich mixtures, the fluid-phase models³ were subsequently supplemented by phase equilibrium calculation methods including solids^{4–6} and hydrates.^{7–9} This mixture model will further be extended with propylene glycol as a suitable candidate for retarding hydrate formation. For this purpose, a fundamental equation of state is needed to represent the

thermodynamic properties of pure propylene glycol at fluid states, which was developed in this work.

A reliable basis of thermal and caloric properties over a broad range of fluid states is essential in fitting equations of state with high demand on validity. To fulfill this need, additional speed-of-sound data were measured with very low experimental uncertainties. In the course of the development of a fundamental equation of state, it is also of special importance to maintain physically correct behavior with a reasonable number of terms.

2. Characteristics of Propylene Glycol

Propylene glycol (C₃H₈O₂, CAS No. 57-55-6), also known as 1,2-propanediol, is a synthetically produced organic compound. With its two hydroxyl groups, it can be assigned to the group of diols. The pure compound is a viscous and highly hygroscopic liquid and is miscible with water, acetone, and chloroform. Propylene glycol is not toxic for humans or animals due to its harmless metabolic by-products, mainly consisting of lactic or pyruvic acid.¹⁰ The center carbon atom of the propylene glycol structure is seen as chiral or asymmetric because of its four different bonds and determines the number of two enantiomers of propylene glycol. Propylene glycol is most commonly manufactured from the noncatalytic hydrolysis of propylene oxide under pressures of 2 MPa and temperatures from 120 to 190 °C. The broad application as an antifreeze is based on the cryoprotective properties of the pure compound as well as the aqueous solution. These properties are related to the absence of any crystal-like structure in the glassy state up to concentrations of 68 wt. % propylene glycol in an aqueous solution.¹¹ The glass-transition behavior and, by implication, the glass-transition temperature T_G are dependent on cooling or warming rates, how the glassy state was formed, and the amount of contained water. An aqueous solution of 45 wt. % liquid propylene glycol changes to glassy at -107.5 °C with a cooling rate of 2.5 K/min.¹¹ According to its antifreeze properties, propylene glycol is often applied in cooling processes as a low-temperature heat transfer fluid. Furthermore, accompanied by its non-toxic character, propylene glycol is broadly applied in the food industry, pharmaceuticals, and cosmetics.

Propylene glycol molecules have strong associative interactions due to their two hydroxyl groups. Since propylene glycol is highly hygroscopic, it is often found in an aqueous solution where it shows a clear affinity to be hydrated, rather than to be self-associated. The new approaches in assessing the association of propylene glycol used by Rhys *et al.*¹² yield a peak of hydroxyl group interactions between two molecules in a 30 mol % aqueous solution at intermolecular or group distances of around 1.95 Å. Taking this into account, pure propylene glycol, without any contribution of hydration, is likely to have a strong associative character. Due to its hygroscopic character, propylene glycol, and glycols in general, are used in the natural gas industry in water-removing processes.

Although propylene glycol is an important fluid in a wide range of applications, it is still not sufficiently investigated. In order to develop mixture models, often involving water or carbon dioxide, highly accurate calculations of properties from a reliable equation of state for pure propylene glycol are needed.

Modern fundamental equations of state are formulated in terms of the Helmholtz energy, which allows the calculation of all thermal and caloric properties directly from combinations of the partial

derivatives of the Helmholtz energy with respect to the independent variables temperature and density. For the development of a fundamental equation of state, a sufficiently wide range of fluid states needs to be covered by experimental measurements. In this work, a new equation of state was developed under consideration of available literature data as well as our own measurements. Table 1 shows the thermodynamic and physical properties of propylene glycol, which are important for the development of its equation.

3. Speed-of-Sound Measurements

The new equation of state for propylene glycol presented here was not only fitted to the available literature data but also to the speed-of-sound data measured in this work. The well-established double-path-length pulse-echo technique was utilized to conduct these measurements in the temperature range from 293.2 to 353.2 K at pressures up to 20 MPa. This dataset is supposed to confirm the speed-of-sound measurements in pure propylene glycol that were carried out by Dávila *et al.*¹⁶ in similar ranges of temperature and pressure.

3.1. Apparatus description

The speed-of-sound measurements were carried out with the double-path-length pulse-echo technique. The apparatus was set up by Gedanitz *et al.*¹⁷ according to the design of Meier and Kabelac¹⁸ and was optimized by Wegge¹⁹ and Wegge *et al.*²⁰ These publications provide more detailed information on the measuring technique and the apparatus. As a brief explanation, the acoustic sensor consists of two polished stainless steel reflectors with an eccentrically attached piezoelectric x-cut quartz crystal. Two different path lengths of $L_1 = 20$ mm and $L_2 = 30$ mm appear. The piezoelectric quartz transducer is excited at its carrier frequency of 8 MHz, with a waveform generator (Agilent Technologies, type: 33220A, USA), which compiles a 30-cycle sinusoidal burst that is further modulated by a half-cycle sine²-function. The ultrasonic pulse is coupled into the fluid and propagates until it reaches the two reflectors and is returned to the quartz crystal that is simultaneously used as the emitter and receiver. Due to the different path lengths, two echoes separated by a time difference Δt_{echo} are captured by a digital oscilloscope (Agilent Technologies, type: MS6032A, USA). The waveform was averaged from 16 consecutive pulses and applied with a bandpass filter based on a fast-Fourier transformation with a bandwidth of 1.6 MHz in order to enhance the signal-to-noise ratio. The time difference Δt_{echo} between the first and second echoes is computed on the basis of the processed data at each state point according to the algorithm described by Dubberke *et al.*,²¹ while the two path lengths are assumed to be constant for a series of measurements. The speed of sound can be determined by the following equation:

$$w = \frac{2 \cdot (L_2 - L_1)}{\Delta t_{\text{echo}} + \tau} \quad (1)$$

According to Harris,²² a correction value τ is considered in order to evaluate the time difference between the ideal-plane wave and the real case. The determination of this correction is described in detail by Gedanitz.²³

The acoustic sensor comprising the quartz transducer and the two reflectors is housed in a stainless steel pressure vessel. A glass feedthrough is implemented to connect the sensor within the pressure vessel and the electronic devices outside. The entire pressure vessel is

TABLE 1. Molar mass and characteristic thermodynamic properties of propylene glycol and the universal gas constant

Physical properties	Denotation	Value	Unit	Reference
Critical temperature	T_c	674.0	K	This work
Critical density	ρ_c	4.46	mol dm^{-3}	This work
Critical pressure	p_c	7.291 8	MPa	This work
Normal-boiling-point temperature	T_B	461.224	K	This work
Triple-point temperature	T_{tr}	242.8	K	Howard ¹³
Liquid density at triple point	$\rho_{tr,liq}$	14.113	mol dm^{-3}	This work
Glass-transition temperature	T_G	169.15 ^a	K	Boutron and Kaufmann ¹¹
Molar mass	M	76.094 42	g mol^{-1}	Wieser and Berglund ¹⁴
Universal gas constant	R	8.314 462 618	$\text{J mol}^{-1} \text{K}^{-1}$	CODATA ¹⁵

^aGlass-transition temperature for pure propylene glycol at a warming rate of 2.5 K min⁻¹.

immersed in a calibration bath thermostat (Fluke, type: 7060, Everett, WA, USA) filled with an ethylene glycol + water mixture. Stable temperature conditions in the range from 293 K to 353 K can therefore be guaranteed. The temperature inside the pressure vessel is measured by a long-stem 25 Ω standard platinum resistance thermometer (SPRT, Rosemount Aerospace, type: 162CE, USA) calibrated on the ITS-90 and connected to a direct current thermometry bridge (Isotech, type: TTI-2, UK). The standard uncertainty for the temperature measurement was $u(T) = 0.004$ K. The pressure measurement is implemented with two vibrating-quartz-crystal pressure transducers (Paroscientific, type: 1000-500A and 1000-6K, USA) that cover different ranges of pressure. The utilization of a differential pressure indicator (Rosemount, type: 3051, USA) to separate the measuring cell and the pressure measuring circuit is crucial to avoid contamination of the pressure transducers with the respective liquid sample. The standard uncertainty for the pressure measurement was $u(p) = 0.0024$ MPa. Both the pressure transducers and the differential pressure indicator are tempered by a second circulation bath thermostat, which operates with deionized water.

3.2. Calibration

In order to determine the speed of sound according to Eq. (1), the time difference between two echoes is measured at each state point. In addition, the difference between the two path lengths needs to be accurately known for a series of measurements since it has a direct impact on the measurement result. However, changes in path length could occur with varying temperature and pressure due to thermal expansion or compression. For those reasons, calibration with purified water was performed to determine the actual difference in path lengths, which is discussed in detail in a previous work by Wegge *et al.*²⁰ Water is a suitable fluid for the calibration procedure since its speed of sound is well known over a wide temperature and pressure range due to highly reliable literature data, such as the datasets by Del Grosso and Mader²⁴ and Fujii and Masui,²⁵ along with an available reference equation of state with very low uncertainty from Wagner and Pr \ddot{u} ß.²⁶ Speed-of-sound measurements in high-purity water were carried out at ten state points at $T = 274.2, 278.2, 283.2, 293.2, 303.2, 313.2, 323.2, 333.2, 343.2,$ and 353.2 K and ambient pressure. The relative deviations of the measured speed of sound in water from values calculated with the IAPWS-95 formulation of Wagner and Pr \ddot{u} ß²⁶ are plotted vs temperature in Fig. 1. With the adjusted path length

difference at reference temperature and one adjusted thermal expansion coefficient linear in temperature, all experimental speed-of-sound data are within the uncertainty of this equation of state, which was estimated to be 0.005% from the equation of state of Wagner and Pr \ddot{u} ß²⁶ in the observed temperature range. In addition, the speed-of-sound data of water measured in the scope of the present work are in good agreement with the reference datasets of Fujii and Masui²⁵ and Del Grosso and Mader²⁴ and show a similar trend compared to the IAPWS-95 formulation (see Fig. 1).

3.3. Measurement fluid

The experimental samples are specified and described in Table 2. Water and propylene glycol are both supplied in glass bottles and need

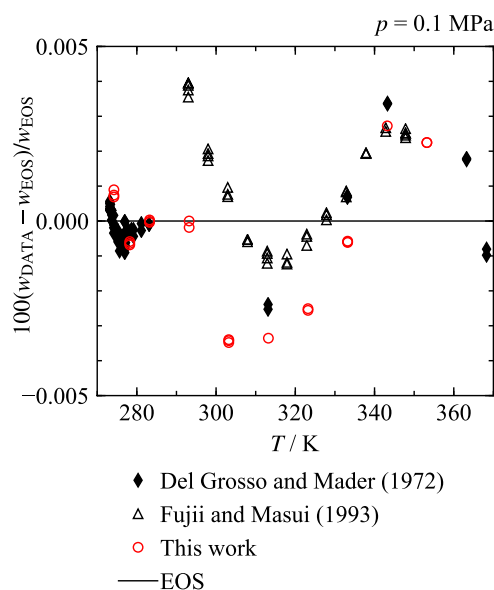


FIG. 1. Results of the calibration speed-of-sound measurements in pure water. The relative deviations of the experimental speeds of sound w_{DATA} from values calculated with the equation of state of Wagner and Pr \ddot{u} ß w_{EOS} at 0.1 MPa are plotted vs temperature. The equation of state is represented by the zero line and has a relative expanded uncertainty of $\pm 0.005\%$ ($k = 2$).

TABLE 2. Sample information of the used experimental materials

Chemical name	Source	CAS number	Purity/mole fraction	Further purification	Analysis method
Water	Sigma-Aldrich	7732-18-5	0.999 997	Degassed	...
Propylene glycol	Sigma-Aldrich	57-55-6	0.998 4	Degassed	Gas chromatography

to be decanted into stainless steel sample cylinders, which can be attached to the sample manifold of the apparatus.

The sample of water was transferred to the sample cylinder at ambient conditions and was further degassed by several freeze-pump-thaw cycles. For this purpose, the sample cylinder is stepwise immersed into liquid nitrogen in order to freeze the liquid phase of water from the bottom to the top. At the same time, impurities involved in the decanting process, such as nitrogen, argon, or oxygen, remain gaseous and detach from the liquid into the upper part of the cylinder. Those gaseous substances are removed by applying a vacuum to the system. The freeze-pump-thaw cycles are repeated until a steady vacuum pressure is reached.

Since propylene glycol has a hygroscopic behavior, the transfer of the sample could not be carried out under ambient conditions. Therefore, the decanting of the propylene glycol sample was performed within the inert, dry atmosphere of a glove-box (MBraun, type: UNILab Plus, Garching, Germany) to avoid contact with atmospheric humidity. Subsequently, the sample of propylene glycol was degassed according to the procedure described above.

The measurement fluid was selected with impurities as low as possible since the quality and accuracy of the obtained speed-of-sound data as well as the related uncertainty of the measurements are significantly dependent upon the purity of the sample fluid.

The purity of the propylene glycol sample was stated by the supplier (Sigma-Aldrich, Burlington, USA) to be at least as good as 99.96 peak area %, investigated by gas chromatography analysis. However, a gas chromatograph requires a calibration to particular standards of well-known compositions in order to provide a quantitative analysis, which had not been conducted here. Thus, the effect of typical impurities of the propylene glycol sample was investigated by assuming that the remaining fraction is entirely dominated by the respective impurity. Water was found to be the impurity that affects the results of the measurements the most, and the purity of propylene glycol was determined to correspond to 99.84 mol %. Since no mixture model for the system propylene glycol + water is available in the literature, the contribution of the sample impurity to the experimental uncertainty was calculated with the reference equation of state of water²⁶ and the present equation of state for propylene glycol combined with a linear mixing rule.

3.4. Experimental procedures

The propylene glycol sample is filled in a cylinder (see Sec. 3.3) that is attached to the sample manifold of the apparatus. In order to remove any remaining substances in the speed-of-sound apparatus, the whole system was evacuated through a cooling trap for several days, with the set-point temperature of the bath thermostat set to the highest possible temperature of 353 K. To achieve a reasonable filling of the apparatus, a heating cable was used to heat up the sample cylinder to ~308 K while the bath thermostat was set to the lowest possible temperature of 253 K. Thus, the filling of the evacuated system could be realized by taking

advantage of the temperature and pressure gradient as well as by support of a hand pump. Subsequently, the temperature of the bath thermostat was set to the lowest measuring temperature at 293 K and the hand pump was used to increase the pressure up to the highest desired value of the first state point. It was not possible to conduct measurements below a temperature of 293 K due to the increasing sound absorption of propylene glycol with decreasing temperature, which led to damping of the acoustic wave. Measurements were performed at equilibrium. The speed-of-sound measurements were carried out along isotherms, starting with the lowest temperature at 293 K and the highest pressure (20 MPa). The adjustment of the following state point was reached by decreasing the pressure with the aid of the hand pump over a 2-h equilibration time. After the completion of one isotherm, the temperature was increased, followed by increasing the pressure with the hand pump to the highest possible value. Measurements were conducted over a temperature range from 293.2 to 353.2 K at pressures up to 20 MPa.

3.5. Results

The speed of sound in propylene glycol was measured over the temperature range from 293.2 to 353.2 K at pressures up to 20 MPa. The measurements were conducted along four isotherms at 293.2, 313.2, 333.2, and 353.2 K with six state points each at 20.0, 15.0, 10.0, 5.0, 2.5, and 0.5 MPa, which led to a total of 24 (p, w, T) data points. At each state point, three measurements were carried out over a period of 1 h in order to confirm the measurements and to investigate the short-time repeatability.

In Fig. 2, the speed of sound is plotted vs pressure. State points with the same temperature are connected to visualize the course of

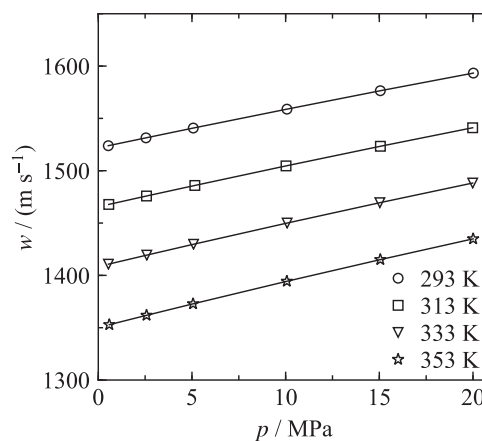


FIG. 2. Speed-of-sound measurements in propylene glycol as a function of pressure along four isotherms. Lines are only shown to guide the eye.

TABLE 3. Speed-of-sound measurements in propylene glycol carried out with the pulse-echo sensor

T (K)	p (MPa)	w (m s ⁻¹)	$U_r(w)$ (%)
293.202	20.020	1593.294	0.029 78
293.202	15.053	1576.429	0.029 78
293.202	10.069	1558.840	0.029 79
293.202	5.070	1540.767	0.029 79
293.202	2.545	1531.412	0.029 79
293.203	0.535	1523.903	0.029 79
<hr/>			
313.202	19.982	1541.057	0.029 79
313.202	15.057	1523.365	0.029 79
313.202	10.020	1504.612	0.029 79
313.202	5.153	1485.924	0.029 80
313.202	2.573	1475.843	0.029 80
313.202	0.560	1467.805	0.029 80
<hr/>			
333.204	19.984	1488.229	0.029 79
333.204	15.030	1469.455	0.029 80
333.204	10.080	1450.003	0.029 80
333.204	5.082	1429.738	0.029 81
333.204	2.588	1419.358	0.029 81
333.204	0.542	1410.713	0.029 82
<hr/>			
353.204	20.008	1434.907	0.029 80
353.204	15.054	1415.063	0.029 81
353.204	10.062	1394.357	0.029 81
353.204	5.060	1372.816	0.029 82
353.204	2.575	1361.835	0.029 83
353.204	0.588	1352.880	0.029 83

each isotherm. The speed of sound decreases with increasing temperature and decreasing pressure. Furthermore, the course of the four isotherms is nearly linear and parallel to each other and there are no intersections among them. The numerical values of the measured sound speeds are listed in Table 3, including temperature, pressure, and relative combined, expanded uncertainty ($k = 2$). Further discussions of the results with comparison to the equation of state and to other data from the literature, such as the datasets of Zorębski *et al.*²⁷ and Dávila *et al.*,¹⁶ are given in Sec. 9.3.

The relative combined expanded uncertainty ($k = 2$) for the measurements in propylene glycol was estimated to be 0.030%

TABLE 4. Uncertainty budget for the speed-of-sound measurements in propylene glycol

Source of uncertainty	Expanded uncertainty	Distribution	Coverage factor	Sensitivity coefficient	Standard uncertainty (%)
Sound-speed measurement	0.010%	Normal	2	1	0.0050
Short-term repeatability	0.002%	Normal	1	1	0.0020
Temperature measurement	8 mK	Normal	2	$(\partial w/\partial T)_p^a$	0.0001
Pressure measurement	0.004 92 MPa	Normal	2	$(\partial w/\partial p)_T^a$	0.0001
Impurities	0.024%	Rectangular	$\sqrt{3}$	1	0.0140
Relative combined, expanded uncertainty ($k = 2$):					0.0298

^aCalculated with the equation of state developed in the scope of this work. The maximum value has been used since the partial derivatives are approximately constant over the investigated temperature and pressure ranges.

following the approach of the previous works by Wegge¹⁹ and Wegge *et al.*²⁰ The uncertainty budget, including temperature and pressure measurements, sound-speed measurements, and short-term repeatability as well as impurities of the material (see Sec. 3.3), is shown in Table 4. The influence of the impurities was the main contribution to the uncertainty and was mainly caused by water, which differs significantly in speed of sound. The supplier also reported water to be the main impurity, and the influence on the uncertainty of the sound-speed measurements was conservatively estimated to be 0.024%.

4. Equation of State

The fundamental equation of state is formulated in terms of the reduced Helmholtz energy, which is a continuous function over the entire fluid region including phase-equilibrium states. The reduced Helmholtz energy α can be derived from its molar form a ,

$$\alpha(\tau, \delta) = \frac{a(T, \rho)}{RT}, \quad (2)$$

with $\delta = \rho/\rho_c$ and $\tau = T_c/T$ as its independent variables. The molar Helmholtz energy is reduced by temperature and the molar gas constant R and is further separated into an ideal (superscript “o”) and a residual (superscript “r”) part,

$$\alpha(\tau, \delta) = \alpha^o(\tau, \delta) + \alpha^r(\tau, \delta). \quad (3)$$

The ideal part α^o describes the hypothetical ideal-gas behavior in the limit of zero density, while the residual part α^r describes the real-fluid deviations from ideal-gas behavior, taking the intermolecular interactions into account.

4.1. Ideal contribution

In the limit of very low density, the real gas behavior is accurately described by the ideal-gas model, since intermolecular forces as well as the molecule’s volume can be neglected. This limiting behavior can be described with the independence of the internal energy U from the volume V ,

$$(\partial U^o/\partial V)_T = 0. \quad (4)$$

Thermal properties can be calculated from the ideal-gas law given by

$$pv = RT. \quad (5)$$

This limiting behavior can be observed for many real gases at moderate and elevated temperatures and low pressures and is thus

valid for broad technical applications. Caloric quantities are calculated from the ideal-gas law in combination with its ideal-gas heat capacity. The dynamic state of a molecule, which can be seen as the internal energy on a macroscopic scale, is responsible for the ideal-gas heat capacity and can be determined from the molecule's intramolecular energies (e.g., translational, rotational, and vibrational). In order to consider the various contributions to the ideal-gas heat capacity independently, a few simplifications and assumptions are usually made when developing an equation of state. Detailed information on the so-called "rigid-rotator, harmonic oscillator" model is given by Lucas²⁸ and summarized in the following. To a considerable degree of accuracy, coupling effects between rotation and vibration within the molecule are negligible. It is further assumed that the whole mass is concentrated in the atomic nuclei and that the masses of the electrons can therefore be neglected. This assumption permits a separate investigation of the electronic energy.

The contribution of translation depends on the atom's translational degrees of freedom, which are determined by three spatial directions. For temperatures greater than 10^{-10} K, all three degrees are assumed to be fully excited. The translational energy of a molecule is originally derived from Schrödinger's equation considering the likelihood of residence of one atom for various quantum numbers and three directions of motion. Since intermolecular forces are not considered in the ideal-gas model and molecules are assumed to be indistinguishable, the subdivision of the system's total translational energy is permissible and, accordingly, so is the summation of all partial energy states to the molecular partition function. The molecular partition function is connected to the thermodynamic function of the system's internal energy, which yields, for the translational contribution to the isochoric heat capacity,

$$\frac{c_{v,\text{trans}}^{\circ}}{R} = \frac{3}{2}. \quad (6)$$

The contribution of the rotational energy to the ideal-gas heat capacity is derived from the kinetic energy of rotation in terms of the principal moments of inertia. Simplifying the molecule's rotational kinetics by considering it to be rigid yields good agreement with reality at normal temperatures. For temperatures much higher than the characteristic temperature of rotation in a linear molecule, the contribution of rotational energy is independent of molecular species and temperature. The characteristic temperatures of external rotation²⁸ in a non-linear molecule are formulated with regard to the associated axes of rotation and are anti-proportional to the related moments of inertia. For a non-linear molecule such as propylene glycol, moments of inertia are not vanishing and thus contribute to the molecular partition function of external rotation.²⁸ Each mode is assumed to be fully excited at temperatures far beyond the characteristic temperature of rotation, which is on the order of a few 10 K depending on the investigated substance. Therefore, it contributes $1/2 R$ to the ideal-gas heat capacity. The non-linear propylene glycol molecule is excitable in three rotational directions and, thus, yields

$$\frac{c_{v,\text{rot}}^{\circ}}{R} = \frac{3}{2}. \quad (7)$$

During vibration, the atoms vibrate around their equilibrium position at which the intramolecular energy reaches its minimum. The intramolecular energy only depends on the distance between

atoms and can thus be associated with intramolecular work, determining the frequency of the vibrational motion.²⁸ To simplify the quantum mechanical analysis, the model of the harmonic oscillator is used to describe the vibration of the diatomic type. Lucas²⁸ provides further information about the relation between the energy states of a linear harmonic oscillator and the vibrational quantum numbers of a diatomic molecule. In the consideration of polyatomic molecules, the complex vibrational structure is transferred to a number of diatomic vibrational motions, introducing the normal coordinate analysis. The intramolecular potential energy can be written as a sum of quadratic terms as a function of the normal coordinates. Ultimately, it becomes possible to describe the vibrational behavior with a maximum number of $3n - 6$ independent vibrations of the diatomic type, where n is the number of atoms in the molecule. The $3n - 6$ normal modes are related to the fundamental harmonic frequencies, which determine the characteristic temperature of the i th normal mode

$$\theta_{\text{vib},i} = h\nu_{0,i}/k_{\text{B}}, \quad (8)$$

where $\nu_{0,i}$ is the fundamental harmonic frequency of the i th normal mode and h and k_{B} are Planck's and Boltzmann's constants, respectively. The molecular partition function, from which the vibrational contribution to the ideal-gas heat capacity can be obtained, is related to the i th characteristic temperature and is defined as the temperature-dependent part of the ideal-gas heat capacity,

$$q_{\text{vib},i} = \sum_{\nu} \exp[-\nu\theta_{\text{vib},i}/T] = \frac{1}{1 - \exp[-\theta_{\text{vib},i}/T]}. \quad (9)$$

Solving the thermodynamic function for the vibrational contribution of the ideal-gas isochoric heat capacity in Eq. (9) yields

$$c_{v,\text{vib}}^{\circ} = \sum_{i=1}^{I_{\text{PE}}} m_i \left(\frac{\theta_{\text{vib},i}}{T} \right)^2 \frac{\exp(\theta_{\text{vib},i}/T)}{[\exp(\theta_{\text{vib},i}/T) - 1]^2}. \quad (10)$$

Equation (10) is known as the Planck–Einstein form, which includes the temperature dependence of the ideal-gas heat capacity. The parameter m_i considers the contribution of vibrational frequencies with similar characteristic temperatures. The characteristic temperature of the vibrational motions of the molecule $\theta_{\text{vib},i}$ as well as the parameter m_i can be determined spectroscopically but are still treated as empirical parameters in the development of equations of state in order to reduce complexity. Equation (10) is often expanded empirically by simple temperature-dependent monomial terms. These terms are usually used for fitting very limited data of the isochoric heat capacity of the ideal gas but are omitted below because of the absence of data.

Taking all three contributions into account, the isobaric heat capacity for the ideal gas yields

$$\frac{c_p^{\circ}}{R} = \frac{c_v^{\circ}}{R} + 1 = c_0 + \sum_{i=1}^{I_{\text{PE}}} m_i \left(\frac{\theta_{\text{vib},i}}{T} \right)^2 \frac{\exp(\theta_{\text{vib},i}/T)}{[\exp(\theta_{\text{vib},i}/T) - 1]^2}, \quad (11)$$

where $c_0 = 4.0$ refers to translational and rotational contributions for a non-linear molecule. The isochoric heat capacity of the ideal gas is directly related to the second derivative of the reduced Helmholtz energy with respect to the reduced temperature τ ,

$$\left(\frac{\partial^2 \alpha^{\circ}}{\partial \tau^2} \right)_{\delta} = -\frac{c_v^{\circ}}{R\tau^2}. \quad (12)$$

Twofold integration of Eq. (12) yields the Helmholtz energy of the ideal gas,

$$\alpha^o(\tau, \delta) = c^{\text{II}} + c^{\text{I}}\tau + (c_0 - 1)\ln(\tau) + \ln(\delta) + \sum_{i=I_{\text{pol}}+1}^{I_{\text{pol}}+I_{\text{PE}}} m_i \ln\left[1 - \exp\left(\frac{-\theta_i}{T_c}\right)\right]. \quad (13)$$

The integration constants c^{I} and c^{II} describe the caloric properties at the reference state in the Helmholtz-energy equation and its first derivative with respect to τ according to Span.²⁹ The origin of the density dependence $\ln(\delta)$ lies in the formulation of the reduced Helmholtz energy, which is calculated from the internal energy, and the density-dependent entropy. The reference state can be arbitrarily defined. For propylene glycol, the normal boiling point is chosen. At the saturated liquid state and T_B ($p = 1$ atm), the enthalpy and entropy are set to zero considering both the contribution of the ideal part [see Eq. (13)] and the residual part of the reduced Helmholtz energy [see Eq. (14)].

4.2. Residual part

The residual part of the Helmholtz energy describes real-fluid behavior differing from the ideal-gas part. Although certain thermodynamic properties are related to distinct terms of the residual part, its parameters are treated empirically. Generally, the residual part can be defined as

$$\alpha^r(\tau, \delta) = \sum_{i=1}^{I_{\text{pol}}} n_i \tau^{t_i} \delta^{d_i} + \sum_{i=I_{\text{pol}}+1}^{I_{\text{pol}}+I_{\text{Exp}}} n_i \tau^{t_i} \delta^{d_i} \exp(-\delta^{p_i}) + \sum_{i=I_{\text{pol}}+I_{\text{Exp}}+1}^{I_{\text{pol}}+I_{\text{Exp}}+I_{\text{GBS}}} n_i \tau^{t_i} \delta^{d_i} \exp(-\eta_i (\delta - \varepsilon_i)^2 - \beta_i (\tau - \gamma_i)^2). \quad (14)$$

The density exponents d_i and p_i must be positive integers, since derivatives with respect to density have to vanish for $\rho \rightarrow 0$, which represents an ideal gas with no molecular interaction. That means that the density exponents are directly related to the virial coefficients, which are defined in the limit of zero density. The temperature exponents t_i should be positive to avoid an infinite contribution to the Helmholtz energy near 0 K.

Polynomial (Pol) and exponential (Exp) terms are sufficient to describe the fluid behavior for most states. Nonetheless, these terms fail near the critical region to give the required accuracy. Thus, additional terms are needed to both yield larger gradients of derivatives of the Helmholtz energy and leave the non-critical region unaffected. For this purpose, Gaussian bell-shaped (GBS) terms were first introduced by Haar *et al.*³⁰ and later adjusted by Setzmann and Wagner³¹ with remarkable accuracy in representing thermal and caloric properties in the critical region. The number of GBS terms is usually kept in the range of 3–7.

5. Fitting Procedure

Fitting a fundamental equation of state is a process that adjusts the equation parameters so that experimental data are reproduced as accurately as possible while maintaining a physically correct behavior of the equation of state. To reach this aim, the influence of each

parameter on certain thermodynamic properties is of major interest for the correlator, as well as the consideration of rough guidelines for temperature and density exponents, as explained in Sec. 4.2.

Reducing the flexibility of the functional form, such as limiting the number of terms, can help obtain suitable physical behavior and reasonable extrapolation. On the other hand, reducing the number of adjustable parameters may hamper the representation of the experimental data. Therefore, a compromise has to be found to fulfill both requirements. To obtain a highly accurate equation of state, it is important to adjust different properties over a broad range of temperatures and pressures. The quality of the datasets used is most important since all properties (e.g., speed of sound and heat capacity) are directly linked and, thus, influence the behavior of other properties. The equation of state should ideally represent all data within their experimental uncertainties. Since measurements are difficult to carry out at low temperatures or very high temperatures and pressures, as well as in the critical region, constraints can be used to ensure correct physical extrapolation of the equation of state.

The difference is the way experimental data are used and correlated. The advantage of nonlinear fitting is the ability to use all properties as an input, without any transformation, whereas with linear fitting, preliminary equations are needed to obtain the independent variables of density and temperature (in the case of the Helmholtz energy) from measured properties such as pressure and temperature. Furthermore, any parameter such as the power in polynomials or the parameters in exponential functions can be directly adjusted. Finally, nonlinear fitting procedures can control the physical behavior of any calculated thermodynamic property, since constraints, including inequality criteria, can be used.

In the process of developing the equation of state for propylene glycol, an error function is used, which differs from the least-squares algorithm. The input objective function f is

$$f = W_x \cdot F_x \quad (15)$$

and can be further mathematically modified. F_x incorporates the deviations between measurement and calculation of thermodynamic properties of each experimental state point (E), along with the contributions from constraints (C), limits (L), and boundaries of a fitted parameter (B). W_x is the weight of each data point (E, C, L, and B) used in the fitting process, and the deviation F_x is defined by

$$F_x = \frac{x_{\text{E,C,L,B}} - x_{\text{EOS}}}{x_{\text{E,C,L,B}}}. \quad (16)$$

The common objective function in conventional minimization problems is the sum of squares. For the development of the present equation of state, it was modified by Gao and Lemmon³² so that not only the square power but also other mathematical functions of logarithmic or exponential forms can be used. The objective function shape can be independently defined for experimental data, constraints, limits, and boundaries such that errors can be minimized and considered differently. In this way, there is higher flexibility when solving multidimensional minimization problems.

During the fitting procedure, the adjustable parameters of the equation of state are varied in order to reduce the overall sum of errors of the calculated properties. With a better knowledge of the uncertainties of each dataset, applying higher weights forces the fitting procedure to more closely match particular data points that have low uncertainties. Although underlying data can be represented correctly

by the equation of state, it might still fail close to phase boundaries or in the critical region due to incorrect physical behavior. Incorrect behavior can be easily detected by unreasonable shapes of the thermodynamic diagrams, for instance, by abrupt changes in various isolines. Consequently, both the deviations of data points and paths of thermodynamic properties must be considered simultaneously. The use of constraints helps control extrapolation by creating barriers for slopes, curvatures, or even higher derivatives and by shaping the isotherms or saturation lines to their correct form. The challenge in applying constraints to obtain a specific shape lies with the assumption of the correct behavior of thermodynamic properties for the particular fluid being fitted in regions where no experimental data are available. To predict certain behavior of properties, the correlator requires a comprehensive knowledge on thermodynamic properties and possible fluid-specific characteristics. This requirement was one of the most challenging aspects in this work because the physical behavior of propylene glycol significantly differs from the behavior of other well-known fluids due to its special physical characteristics (e.g., strong association or chemical decomposition at temperatures below the critical point).

6. Critical Point Determination

Significant ranges of propylene glycol even at temperatures below the critical point are not investigated experimentally because of the thermal decomposition of the fluid. According to Diaz *et al.*,³³ decomposition due to oxidation reactions happens at temperatures between 400 and 600 K, resulting in acetone, acetaldehyde, formaldehyde, and carbon dioxide via carbon bond cleavage. Even at lower temperatures, some dissociation can be expected. Consequently, the critical properties are difficult to obtain with conventional measurement techniques.

A flow method for the determination of critical data for thermally unstable compounds such as propylene glycol was developed by VonNiederhausern *et al.*³⁴ Estimated critical parameters, obtained by Kazakov *et al.*³⁵ and Carande *et al.*³⁶ from a regression method based on quantitative structure–property relationships (QSPRs), are available and considered in the subsequent discussion.

The measurement of critical temperatures of a thermally unstable compound with a static method requires an unreasonably fast heating rate of the sample to avoid thermal decomposition. The advantage of a flow measurement technique is that accurate temperature scans can be taken over a wide time frame since the temperature bath can be heated smoothly at very low residence times of the samples. To obtain the critical temperature and pressure, several temperature scans close to the critical point must be evaluated. A single, subcritical temperature scan is characterized by a flat, horizontal path of the fluid temperature with simultaneously rising bath temperature, which indicates isothermal boiling at constant pressure. This behavior does not exist above the critical point, where the transition between liquid and gas is indiscernible. Evaluation of several temperature scans at different pressures narrows down the temperature and pressure range in which the critical point is located. The critical point is inferred by the temperature and pressure where isothermal boiling is no longer observed. By varying the flow rates, different critical temperatures can be observed with the estimation method described above since the degree of thermal decomposition depends on the residence time at high temperatures. The reported critical temperature is the extrapolated value at zero residence time, where the extrapolation was obtained from a quadratic fit of the measured data. The numerical values for the critical temperature and pressure are associated with uncertainties of 0.3 K and 0.007 MPa according to VonNiederhausern *et al.*³⁷ This seems small, since VonNiederhausern *et al.*³⁴ already assumed an error in the interpretation of the temperature scans of 1 K and 2% for the critical temperature and pressure. Other contributions such as calibration uncertainties or uncertainties from the mathematical extrapolation procedure also have to be considered. Therefore, the overall uncertainty for the critical data is expected to be significantly higher. Critical densities cannot be obtained with this flow method. The difficulty associated with the method of VonNiederhausern *et al.*³⁴ is getting close to the critical point in the first place. Since this experiment yields measurements associated with rather high uncertainties, estimation methods are also considered here.

TABLE 5. Overview of all experimentally obtained and estimated critical properties of propylene glycol. Indicated uncertainties are reported in the corresponding publications

References	Method	T_c (K)	p_c (MPa)	ρ_c (mol dm ⁻³)
VonNiederhausern <i>et al.</i> ³⁷	Experimental	676.4	5.941	...
Kazakov <i>et al.</i> ³⁵	QSPR	673.2 ± 3.5	6.043 ± 0.209 ^a	...
Carande <i>et al.</i> ³⁶	QSPR	666.8 ± 1.9	5.865 ± 0.336 ^a	...
Joback and Reid ³⁸	GC	626.67 ^b	5.792 ^b	4.246 ^b
Steele <i>et al.</i> ⁴¹	Fitted	676.4 ^c	6.75	4.048
Dean ⁴²	Not stated	625.15	6.08	4.219
Yaws ⁴³	Not stated	626.0	6.1	4.184
Gallant ⁴⁴	Not stated	624.15	6.095	4.218
Wilding <i>et al.</i> ⁴⁵	Not stated	625.6	6.07	...
This work	Fitted	674.0	7.2918	4.460

^aValues for p_c calculated with T_c and T_c/p_c from the work of Kazakov *et al.*³⁵ and Carande *et al.*³⁶ considering the propagation of uncertainty.

^bCalculation rules taken from VDI WärmAtlas.⁴⁶

^cValue for T_c taken from the work of VonNiederhausern *et al.*³⁷ and used in the fitting procedure for p_c and ρ_c .

The most established group contribution (GC) method of Joback and Reid³⁸ is applicable for a broad field of compounds. It is described in Ref. 39 and based on an earlier GC method of Lydersen (1955). However, the applicability of such methods needs to be closely reviewed when determining properties for substances with strong associative character. Propylene glycol is such a substance, which forms clusters of several molecules due to hydrogen bonds. Common GC methods only consider intramolecular group effects. Thus, they might not be suitable for estimating properties of associating, cluster-forming substances. In fact, the critical temperature of propylene glycol estimated by the method of Joback and Reid³⁸ is 626.67 K (see Table 5), which is roughly 50 K below the measured temperature of VonNiederhausern *et al.*³⁷

The principle of the QSPR methods for the estimation of critical parameters is explained in detail by Kazakov *et al.*³⁵ and Carande *et al.*³⁶ They provide detailed information on the theoretical background, methodical procedure, and implementation on the basis of broad underlying datasets. Generally, all QSPR methods are based on a relation between a property of interest and the molecular numerical features derived theoretically from the individual chemical structure of monomers of the considered fluid.

The molecular numerical features are commonly called descriptors and their relationship to the chosen property is established through non-linear regression analysis from broad data collections (cf. Ref. 35). The properties considered in the investigations of Kazakov *et al.*³⁵ and Carande *et al.*³⁶ are the critical temperature T_c , the ratio of the critical temperature and the critical pressure T_c/p_c , and the saturation reduced pressure $p_{v,r}$ at $T/T_c = 0.7$, which is commonly used for the calculation of the acentric factor ω . Kazakov *et al.*³⁵ and Carande *et al.*³⁶ used a support vector machine (SVM) methodology for their regression since it offers several numerical and computational advantages over other methods. With the demand for a very precise adjustment of the support vector regression (SVR) and kernel parameters, the dataset is split into three parts: the training set, the validation set, and the testing set. First, an initial model is generated with a reduced and selected dataset (training set), which is then able to predict the data from the validation set most accurately. Once the optimal model parameters are obtained, the final model is generated with the combined training and validation set (testing set). Kazakov *et al.*³⁵ also provided detailed information on potential model errors of QSPR methods. Accordingly, a significant uncertainty contribution can be caused by uncertainties of the underlying experimental data used to produce the model. In case the predicted properties lie beyond the available data, such as with the critical properties for propylene glycol, and also physical mechanisms such as cluster-forming association are dominating the properties of the fluid, the suitability of the model decreases. The reason for that is the increasing deviation from a monomer-like structure, which is the basis of the structure input. With increasing associative behavior, the physical mechanisms are predominantly characterized by mixtures of monomers, dimers, and larger clusters. In fact, Kazakov *et al.*³⁵ named two example fluids, propylene carbonate and γ -butyrolactone, with outlier characteristics in the estimated critical temperatures, which are predominantly caused by association.

Considering propylene glycol as an associative and linear-structured fluid, the uncertainty caused by association results in a noticeable deviation of the QSPR-predicted values from the

underlying experimental data obtained from VonNiederhausern *et al.*³⁷ Taking into account that predictions for the critical temperature of propylene glycol need to be extrapolated about 200 K beyond the available data, the estimation uncertainty obtained from QSPR-SVM is expected to gradually increase toward the critical point. Compared to GC-based methods, QSPR-SVM models exhibit better performance in approaching the experimentally obtained critical parameters of propylene glycol (see Table 5). Nonetheless, the predictions of Kazakov *et al.*³⁵ and Carande *et al.*,³⁶ who used an enhanced number of descriptors and improved datasets, both lack in the accurate prediction of the critical parameters due to the unsuitable model basis for associating fluids.

All QSPR and GC-based estimations of the critical parameters for propylene glycol are shown in Table 5 along with the experimentally obtained data of VonNiederhausern *et al.*³⁷

The critical parameters of an equation of state define the shape of the saturated liquid and vapor curves as well as slopes and curvatures of, e.g., isotherms in a pressure–density plot. Therefore, the choice of the critical parameters has a significant influence on the representation of experimental densities. Since the critical temperature of VonNiederhausern *et al.*³⁷ is the only measurement and it is somewhat confirmed by the QSPR value of Kazakov *et al.*,³⁵ $T_c = 676.4$ K was used as the starting point in the fitting procedure. During the fit, it was slightly modified so that the accurate density measurements of Sampson *et al.*⁴⁰ could be reproduced more accurately and the critical density was simultaneously adjusted. The critical pressure was calculated from the present equation of state. The final values used for the present equation of state are listed in Tables 1 and 5.

7. Isobaric Heat Capacity of the Ideal Gas

As mentioned in Sec. 4.1, the ideal part of the equation of state is required for the calculation of caloric properties. It is subject to the temperature-dependent part of the ideal-gas heat capacity, which is defined by the intramolecular forces of the molecule. The process of developing the ideal part of the equation of state for propylene glycol was particularly challenging since no data for the ideal-gas isobaric heat capacity are available in the literature. Therefore, the GC method

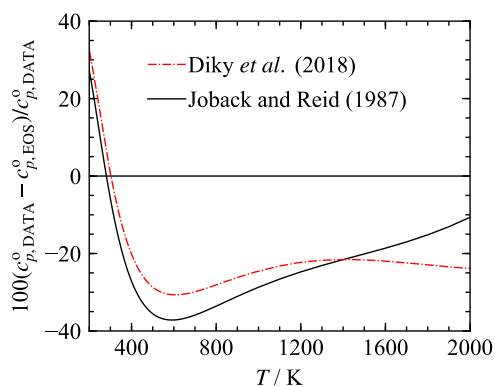


FIG. 3. Deviations of the calculated ideal-gas isobaric-heat-capacity data from the equation of state.

TABLE 6. Parameters of the Planck–Einstein terms of the ideal part of the equation of state according to Eq. (17)

i	m_i	θ_i (K)
1	5	1000
2	28	1330

of Joback and Reid,³⁸ presented in the VDI Wärmeatlas,⁴⁶ was used to estimate values. However, due to the same limitations as explained in Sec. 6, the data turned out to be not useful for the fitting process.

In the course of new software implementations and model developments of the Thermo Data Engine (TDE),⁴⁷ the TDE software developers have made progress in predicting ideal-gas heat capacities at constant pressure for associating fluids. Although not yet published, the dataset for the ideal-gas heat capacity of propylene glycol of Diky *et al.*⁴⁸ is investigated with respect to its deviations from the present equation of state along with the data obtained from the GC method of Joback and Reid;³⁸ see Fig. 3.

The predictions of Diky *et al.*⁴⁸ match the present equation of state only slightly better than the data calculated with the GC approach of Joback and Reid.³⁸ Therefore, both datasets are considered as unsuitable for the development of the present equation of state. Another approach had to be used to derive the ideal gas part of the reduced Helmholtz energy.

8. Equation of State for Propylene Glycol

The ideal part of the equation of state is based on the isobaric heat capacity of the ideal gas. The ideal-gas isobaric heat capacity is

generally constructed with Planck–Einstein and monomial terms [cf. Eq. (13)]. For modern equations of state, monomial terms are not considered anymore due to challenging extrapolation behavior. The ideal part of the equation of state for propylene glycol is written as

$$\alpha^o(\tau, \delta) = c^{\text{II}} + c^{\text{I}}\tau + 3 \ln(\tau) + \ln(\delta) + \sum_{i=1}^2 m_i \ln[1 - \exp(-\theta_i\tau/T_c)]. \quad (17)$$

The two integration constants, $c^{\text{I}} = 2.583\,963\,325\,603\,2$ and $c^{\text{II}} = 1.453\,592\,250\,028\,98$, were adjusted so that the molar enthalpy $h_0 = 0$ and molar entropy $s_0 = 0$ for the saturated liquid at the normal boiling point. The parameters of the Planck–Einstein terms in Eq. (17) are listed in Table 6.

The estimated ideal-gas isobaric-heat-capacity data, obtained from the estimation methods, were not considered in the validation of the ideal part of the equation of state due to the issues discussed in Sec. 7. Therefore, the parameters were mainly fitted to reliable speed-of-sound data in the liquid state as well as isobaric-heat-capacity data. This has proven to be a reliable method as described by Lemmon and Span⁴⁹ and Thol *et al.*⁵⁰ They provided the enthalpy of evaporation and its temperature dependence from the Clausius relation with sufficient accuracy.

The residual part of the equation of state for propylene glycol consists of six monomial, six exponential, and seven GBS terms,

$$\alpha^r(\tau, \delta) = \sum_{i=1}^6 n_i \tau^{t_i} \delta^{d_i} + \sum_{i=7}^{12} n_i \tau^{t_i} \delta^{d_i} \exp(-\delta^{p_i}) + \sum_{i=13}^{19} n_i \tau^{t_i} \delta^{d_i} \exp[-\eta_i (\delta - \varepsilon_i)^2 - \beta_i (\tau - \gamma_i)^2]. \quad (18)$$

TABLE 7. Parameters of the residual part of the equation of state for propylene glycol according to Eq. (18)

i	n_i	t_i	d_i	p_i	η_i	β_i	γ_i	ε_i
1	$4.661\,153\,8 \times 10^{-2}$	1.000	4					
2	2.027 399 2	0.140	1					
3	-2.604 866 4	0.920	1					
4	$-5.859\,279\,2 \times 10^{-1}$	1.254	2					
5	$2.967\,405\,0 \times 10^{-1}$	0.425	2					
6	$5.386\,365\,6 \times 10^{-2}$	0.688	3					
7	$-7.828\,092\,4 \times 10^{-2}$	1.600	1	2				
8	$-7.696\,802\,5 \times 10^{-1}$	2.230	3	2				
9	$1.301\,635\,9 \times 10^{-1}$	1.550	2	1				
10	$-1.528\,758\,5 \times 10^{-2}$	0.900	7	1				
11	$-1.000\,001\,5 \times 10^{-2}$	5.000	1	3				
12	$-1.500\,221\,0 \times 10^{-1}$	3.000	2	2				
13	$-2.442\,652\,6 \times 10^{-1}$	1.100	2	2	18.7	685.0	1.090	0.789
14	$-3.567\,370\,0 \times 10^{-2}$	1.000	2	2	18.7	1230.0	1.040	0.990
15	$-2.715\,083\,5 \times 10^{-1}$	1.500	1	2	1.860	2.280	1.050	0.981
16	1.294 829 8	2.440	1	2	0.630	0.130	1.500	1.004
17	-1.703 145 4	2.370	1	2	0.830	0.070	1.430	0.698
18	1.760 046 1	1.770	1	2	1.278	1.090	1.130	0.808
19	-1.065 447 8	2.280	1	2	0.450	0.130	2.110	0.810

TABLE 8. Test values for the verification of computer implementation

T K	$\frac{\rho}{\text{mol dm}^{-3}}$	$\frac{p}{\text{MPa}}$	$\frac{w}{\text{m s}^{-1}}$	$\frac{c_p}{\text{J mol}^{-1} \text{K}^{-1}}$	$\frac{h}{\text{J mol}^{-1}}$	$\frac{s}{\text{J mol}^{-1} \text{K}^{-1}}$	$\frac{a}{\text{J mol}^{-1}}$
400.0	0.001	0.003 322 047 6	214.573 21	158.296 76	43 040.574	119.959 47	-8 265.262 2
400.0	13	61.287 909	1 467.826 7	227.484 03	-11 727.204	-38.665 809	-975.334 62
500.0	0.01	0.041 324 887	237.581 57	197.106 14	60 808.024	138.553 17	-12 601.051
500.0	13	196.801 28	1 633.680 9	252.379 35	19 730.659	8.167 559 9	508.318 41
680.0	13	430.549 03	1 814.610 0	280.864 19	80 765.269	81.467 593	-7 751.850 4

All parameters of Eq. (18) are listed in Table 7.

Considering all underlying data, the lower temperature limit of the equation is the triple-point temperature $T_{\text{tr}} = 242.8$ K. The upper temperature $T_{\text{max}} = 680$ K is chosen to be slightly above the critical temperature. The upper pressure limit of $p_{\text{max}} = 350$ MPa is determined by the dataset of Guignon *et al.*⁵¹ Bridgman⁵² reported density measurements at much higher pressures up to 1177 MPa. They are not considered in the fitting process; however, the equation of state shows a correct extrapolation behavior to fairly high pressures, which is discussed in more detail in Sec. 10.

Table 8 contains test values for the verification of computer implementation of the equation of state.

Ancillary equations for the vapor pressure p_v , the saturated liquid density ρ' , and the saturated vapor density ρ'' are used to estimate starting values for the iterative calculation of properties along the saturation line. Thus, the fitting process of the equation of state as well as the calculation of phase-equilibrium data are expedited perceptibly. The parameters of Eqs. (19)–(21) are listed in Table 9,

$$\ln\left(\frac{p_v}{p_c}\right) = \frac{T_c}{T} \sum_{i=1}^5 n_i \left(1 - \frac{T}{T_c}\right)^{k_i}, \quad (19)$$

$$\frac{\rho'}{\rho_c} = 1 + \sum_{i=1}^5 n_i \left(1 - \frac{T}{T_c}\right)^{k_i}, \quad (20)$$

$$\ln\left(\frac{\rho''}{\rho_c}\right) = \sum_{i=1}^6 n_i \left(1 - \frac{T}{T_c}\right)^{k_i}. \quad (21)$$

Figure 4 shows that deviations between the ancillary equations and the fundamental equation of state are less than 0.07%. Deviations are higher very close to the critical point.

TABLE 9. Parameters of the ancillary equations for the vapor pressure p_v , the saturated liquid density ρ' , and the saturated vapor density ρ'' according to Eqs. (19)–(21)

i	p_v [Eq. (19)]		ρ' [Eq. (20)]		ρ'' [Eq. (21)]	
	n_i	k_i	n_i	k_i	n_i	k_i
1	-0.1012×10^2	1.0	0.4600×10^0	0.21	$-0.205 07 \times 10^1$	0.32
2	0.3150×10^1	1.5	0.2060×10^1	0.43	$-0.683 62 \times 10^1$	0.90
3	-0.5600×10^1	2.6	0.7430×10^0	2.70	$-0.198 35 \times 10^2$	2.50
4	-0.3370×10^0	4.0	-0.1905×10^1	3.70	$-0.100 97 \times 10^2$	4.20
5	-0.2390×10^1	5.0	0.1536×10^1	4.70	$-0.557 72 \times 10^2$	5.70
6					$-0.144 55 \times 10^3$	12.00

9. Comparison with Literature Data and Validation of the Equation of State

The percent deviation of any measured or estimated data point x_{Data} from the calculated property x_{EOS} , obtained from the present equation of state, is defined as

$$\Delta x = 100 \left(\frac{x_{\text{Data}} - x_{\text{EOS}}}{x_{\text{Data}}} \right). \quad (22)$$

A convenient quantity to compare datasets from different sources with respect to their deviations from the equation of state is the averaged absolute relative deviation (AAD),

$$\text{AAD} = \frac{1}{N} \sum_{i=1}^N |\Delta x_i|. \quad (23)$$

In Eq. (23), the quantity N corresponds to the number of data points for each author and property.

The available data for developing the equation of state for propylene glycol were found in 145 publications with measured data as well as estimates. Overall, 1366 data points are available, comprising homogeneous densities, saturated liquid densities, vapor pressures, isobaric heat capacities, sound speeds, and critical parameters. A summary of all data points and the quantity of fitted data points is given in Table 10.

In order to ensure stable and physically correct behavior of the equation of state, the underlying datasets need to represent the fluid states in a broad temperature and pressure range. The quality of datasets is closely related to the quality and the reliability of the equation of state. For the accuracy of the data, the measurement techniques, the purity of the sample, and the uncertainty of the employed apparatus are of great importance. Ideally, reliable uncertainties of the measured quantities are stated in the corresponding publications and can be included in the fitting procedure.

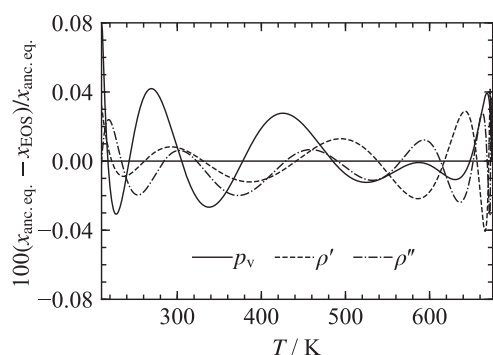


FIG. 4. Deviations of the values calculated with the ancillary equations for the vapor pressure p_v , the saturated liquid density ρ' , and the saturated vapor density ρ'' from the equation of state.

TABLE 10. Summary of all underlying experimental and estimated data points

Property	All available data points	Fitted data points
c_p	73	12
c_p^o	472 ^a	...
$p\rho T$	867	27
ρ'	17	1
p_v	246	5
w	163	20
Total (without c_p^o)	1366	65

^aEstimations of the ideal-gas heat capacity by Diky *et al.*⁴⁸ and Joback and Reid.³⁸

Unfortunately, older publications usually lack such quantifications but are not significantly less likely to contain high-quality data.

Figure 5 illustrates the limited data situation for propylene glycol. Homogeneous thermal and caloric data are restricted to the liquid phase and at temperatures far below the critical state due to the inaccessibility of the gaseous states in experiments at rather low

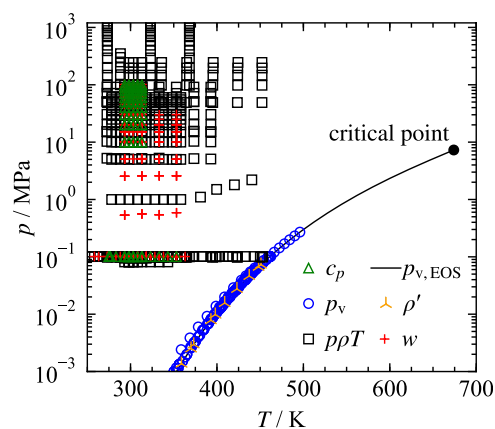


FIG. 5. p, T -diagram with all available data in relation to the vapor-pressure curve and the critical point.

pressures or the thermal decomposition of the sample at elevated temperatures.

9.1. Comparisons of homogeneous density data

The density data for propylene glycol are limited to homogeneous liquid densities within a relatively narrow temperature range, predominantly at ambient pressure; see Table 11. Figure 5 gives an overview of the location of the data in the fluid region.

All data lie within 243 and 453 K, with pressures up to 1177 MPa. Without considering the data of Bridgman,⁵² density data are limited to a maximum pressure of 350 MPa.⁵¹ Due to the thermal decomposition of propylene glycol, thermodynamic properties at elevated temperatures (a rather broad temperature range of 200 K below the critical point) have not been experimentally investigated. This fact as well as the imprecise knowledge of the critical point was a challenge during the fitting procedure.

The data of Sampson *et al.*⁴⁰ were specifically measured for the development of the present equation of state. With 100 state points in a temperature range of 272–393 K and pressures up to 92 MPa, it is the second most comprehensive dataset. The measurements were carried out with a commercial high-pressure vibrating-tube densimeter (VTD) model DMH HPM manufactured by Anton Paar, Graz, Austria. The vibrating-tube measurement is based on the relation between the density and the vibration period of a U-shaped tube, which is measured by a frequency counter according to Kayukawa *et al.*⁹⁰ Before the actual measurement, the VTD was calibrated at temperatures between 283 and 383 K with pressures up to 98 MPa. The substances used for the calibration were water and helium, which are typical compounds for this purpose. The liquid-phase densities of propylene glycol and water are similar, whereas helium is used as a fixed point at comparatively low densities. From two underlying models of Outcalt and McLinden⁹¹ and May *et al.*,⁹² a very accurate calibration correlation was obtained. Sampson *et al.*⁴⁰ estimated the relative combined expanded uncertainty to be within 0.15% (1.56 kg m^{-3}), considering uncertainties of temperature, pressure, oscillation period, and calibration, as well as sample impurities of 99.5 mol % for a degassed sample. Each single data point is represented by the equation of state with a deviation of less than 0.05% (cf. Fig. 6), which is well within the specified uncertainties. In fact, the uncertainty estimate of the measurements seems to be very conservative to us.

For overlapping temperature ranges, the data of Sampson *et al.*⁴⁰ show good agreement with another comprehensive dataset obtained by Zorębski *et al.*²⁷ These data are derived from the accurate speed-of-sound measurements presented in the same paper. The procedure is based on the approach of Sun *et al.*⁹³ When performed correctly, this leads to very accurate results, sometimes better than would be possible with direct density measurements.^{93–95} The dataset includes 73 data points in a temperature range of 283–364 K with fairly high pressures up to 100 MPa and the respective uncertainties are claimed to be 0.02%. The deviations of the data from the equation of state are within this range for most state points within 298–364 K. At lower temperatures, deviations increase up to 0.06%.

The homogeneous density measurements of Bridgman⁵² cover pressures up to 1177 MPa. According to Bridgman,⁵² the measured densities are subject to an error in connection with thermal expansion, which, however, is negligibly small taking other uncertainties such as impurities of the sample into account. The data were not used

TABLE 11. Summary of available homogeneous liquid density data along with the temperature and pressure ranges and their overall AADs with respect to the equation of state. For a better overview, datasets with fewer than five data points are summarized and labeled as “all authors with fewer than five data points” in the last row of the table

Author	Year	<i>N</i>	<i>T</i> (K)	<i>p</i> (MPa)	AAD (%)
Atilhan and Aparicio ⁵³	2013	126	278–359	0.1–60.0	0.043
Bajić <i>et al.</i> ⁵⁴	2013	10	288–334	0.101 325	0.022
Bridgman ⁵²	1932	42	273–369	<0.1–1177	1.2
Domańska <i>et al.</i> ⁵⁵	2014	9	313–354	0.1	0.032
Garber <i>et al.</i> ⁵⁶	1970	5	293.14	0.101 325	0.16
George and Sastry ⁵⁷	2003	5	298–339	0.101 325	0.023
Geyer <i>et al.</i> ⁵⁸	2000	5	278–319	0.101 325	0.064
Geyer <i>et al.</i> ⁵⁹	2001	12	288–309	0.1–60.0	0.026
Guignon <i>et al.</i> ⁵¹	2010	8	288–289	0.1–350	0.24
Jiménez and Martínez ⁶⁰	2005	5	293–314	0.101 325	0.017
Jones and Tamplin ⁶¹	1952	41	273–314	0.101 325	0.030
Khattab <i>et al.</i> ⁶²	2013	7	293–323	0.101 325	0.26
Krishna <i>et al.</i> ⁶³	2015	6	298–324	0.101 325	0.028
Li <i>et al.</i> ⁶⁴	2007	8	298–334	0.101 325	0.052
Li <i>et al.</i> ⁶⁵	2008	8	293–329	0.101 325	0.036
Ling <i>et al.</i> ⁶⁶	2011	6	298–324	0.101 325	0.035
Ling <i>et al.</i> ⁶⁷	2016	6	293–319	0.101 325	0.042
Makarov <i>et al.</i> ⁶⁸	2016	15	274–334	0.1	0.060
Marchetti <i>et al.</i> ⁶⁹	2000	19	263–354	0.101 325	0.036
Nain ⁷⁰	2007	6	293–319	0.101 325	0.049
Olson and Cordray ⁷¹	1992	7	273–419	0.101 325	0.061
Pal <i>et al.</i> ⁷²	2016	6	293–319	0.1	0.043
Ponedelnikova and Tarasova ⁷³	1954	12	258–364	0.101 325	0.066
Rane <i>et al.</i> ⁷⁴	2016	6	293–319	<0.1	0.022
Romero <i>et al.</i> ⁷⁵	2008	6	283–309	<0.1	0.037
Sadykov <i>et al.</i> ⁷⁶	1974	16	302–453	0.101 325	0.24
Sagdeev <i>et al.</i> ⁷⁷	2017	57	293–453	<0.1–246	0.20
Saleh <i>et al.</i> ⁷⁸	1999	5	303–324	0.101 325	0.077
Sampson <i>et al.</i> ⁴⁰	2019	100	272–393	5.0–91.4	0.026
Soldatović <i>et al.</i> ⁷⁹	2016	7	293–324	0.1	0.021
Sun and Teja ⁸⁰	2004	8	298–441	0.1–2.2	0.14
Timmermans and Hennaut-Roland ⁸¹	1955	7	273–304	0.101 325	0.021
Tsai <i>et al.</i> ⁸²	2009	5	303–344	0.101 325	0.059
Vinogradov and Shakhparonov ⁸³	1984	7	243–333	0.1	0.027
Zarei <i>et al.</i> ⁸⁴	2008	7	293–344	<0.1	0.024
Zarei <i>et al.</i> ⁸⁵	2013	6	293–334	0.101 325	0.021
Zemánková <i>et al.</i> ⁸⁶	2013	5	283–314	0.101 325	0.024
Zhuravlev ⁸⁷	1992	19	243–423	0.101 325	0.22
Zhuravlev <i>et al.</i> ⁸⁸	1985	13	243–364	0.101 325	0.066
Zivković <i>et al.</i> ⁸⁹	2014	8	288–324	0.101 325	0.019
Zorębski <i>et al.</i> ²⁷	2008	73	283–364	0.1–100	0.018
All authors with fewer than five data points		138	273–358	<0.1–0.1	0.11

for the development of the equation of state but to verify its extrapolation behavior. The deviations from the equation of state are less than 1.6% (cf. Fig. 7).

Figure 8 shows the deviations of homogeneous liquid density data at atmospheric pressure. Showing good agreement with the dataset of Sampson *et al.*⁴⁰ at elevated pressures, the dataset of Zorębski *et al.*²⁷ is considered as a basis for analysis at atmospheric pressure. Moreover, their data are in good agreement with those

obtained by Zarei *et al.*⁸⁴ and Orge *et al.*⁹⁶ The seven data points of Zarei *et al.*⁸⁴ deviate by less than 0.034% from the equation, which is well in agreement with the deviations of Zorębski *et al.*²⁷ (0.06%) in the corresponding temperature range. Zarei *et al.*⁸⁴ used an Anton Paar DMA 4500 with a certified precision of 0.005 g dm⁻³ and an automatic viscosity correction, but no information on a combined uncertainty is given. The dataset of Bajić *et al.*⁵⁴ shows data conforming to those of Zorębski *et al.*²⁷ within a temperature range of

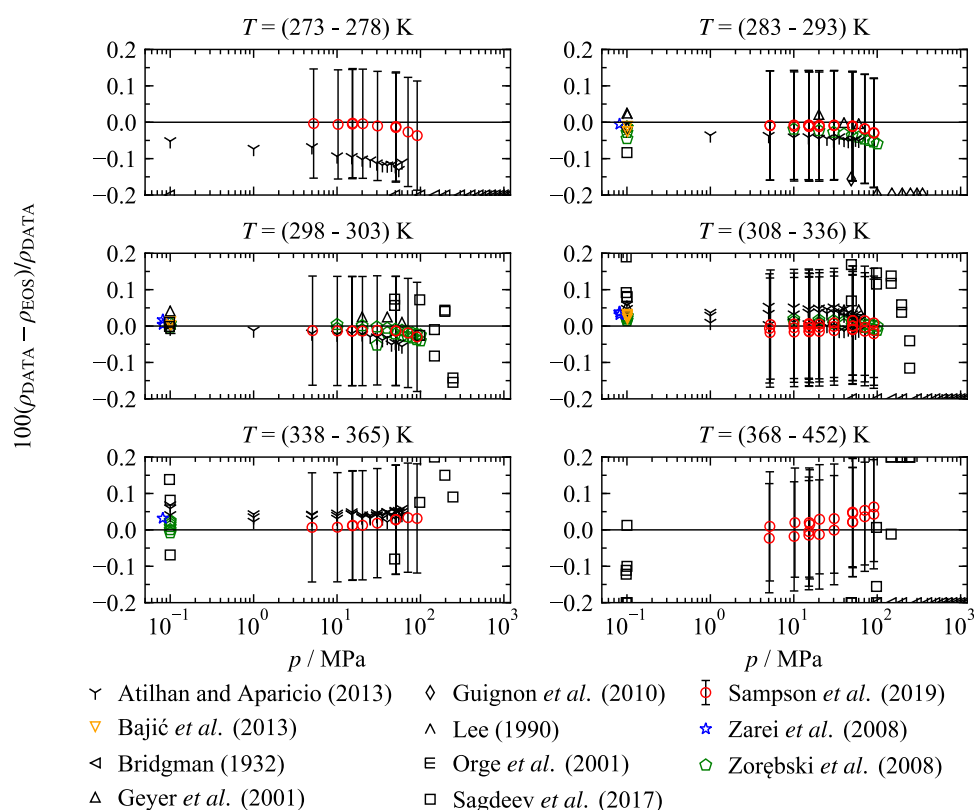


FIG. 6. Deviations of homogeneous liquid density data from the equation of state for selected datasets in selected temperature ranges as a function of the logarithmic pressure.

288–334 K at atmospheric pressure (cf. Fig. 8). They used a similar apparatus and the same calibration procedure as Zarei *et al.*⁸⁴ while claiming a quite optimistic experimental uncertainty of 0.01 kg m^{-3} (0.001%). The measurements are represented with the equation of state within deviations of less than 0.032%.

In Fig. 8, curvature can be observed in the deviations of experimental data from the equation of state. Nonetheless, the

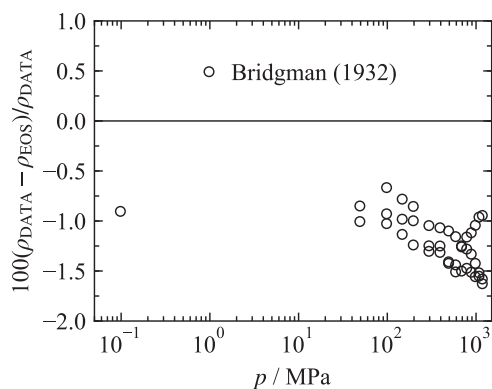


FIG. 7. Deviations of homogeneous liquid density data of Bridgman⁵² from the equation of state as a function of the logarithmic pressure.

deviations from the equation of state of the majority of the datasets are still within 0.05% and, thus, represented within a reasonable range of uncertainty. In the course of the fitting process, the curvature was accepted in order to achieve a better representation of the data in the low-temperature region ($T < 270 \text{ K}$). A compromise was made so that the data of Vinogradov *et al.*⁸³ and Zhuravlev *et al.*^{87,88} are represented within 0.07%. However, to give a more reliable statement to define which low-temperature data should be fitted, further experimental investigations are required.

Based on the above discussion, uncertainties of densities calculated with the present equation of state at atmospheric pressure are estimated to be 0.06% at temperatures between 270 and 380 K. At lower temperatures, uncertainties increase up to 0.1%. The uncertainty of calculated densities at elevated pressures is estimated to be 0.06% between 270 and 460 K and pressures up to 100 MPa based on the data of Sampson *et al.*⁴⁰ and Zorębski *et al.*²⁷

9.2. Comparisons of vapor-liquid equilibrium data

In addition to a close investigation of the homogeneous liquid density datasets, several vapor pressure as well as saturated liquid density datasets are compared with respect to their representation with the equation of state. The collected datasets, including 246 vapor pressure and 17 saturated liquid density measurements, are presented in Table 12.

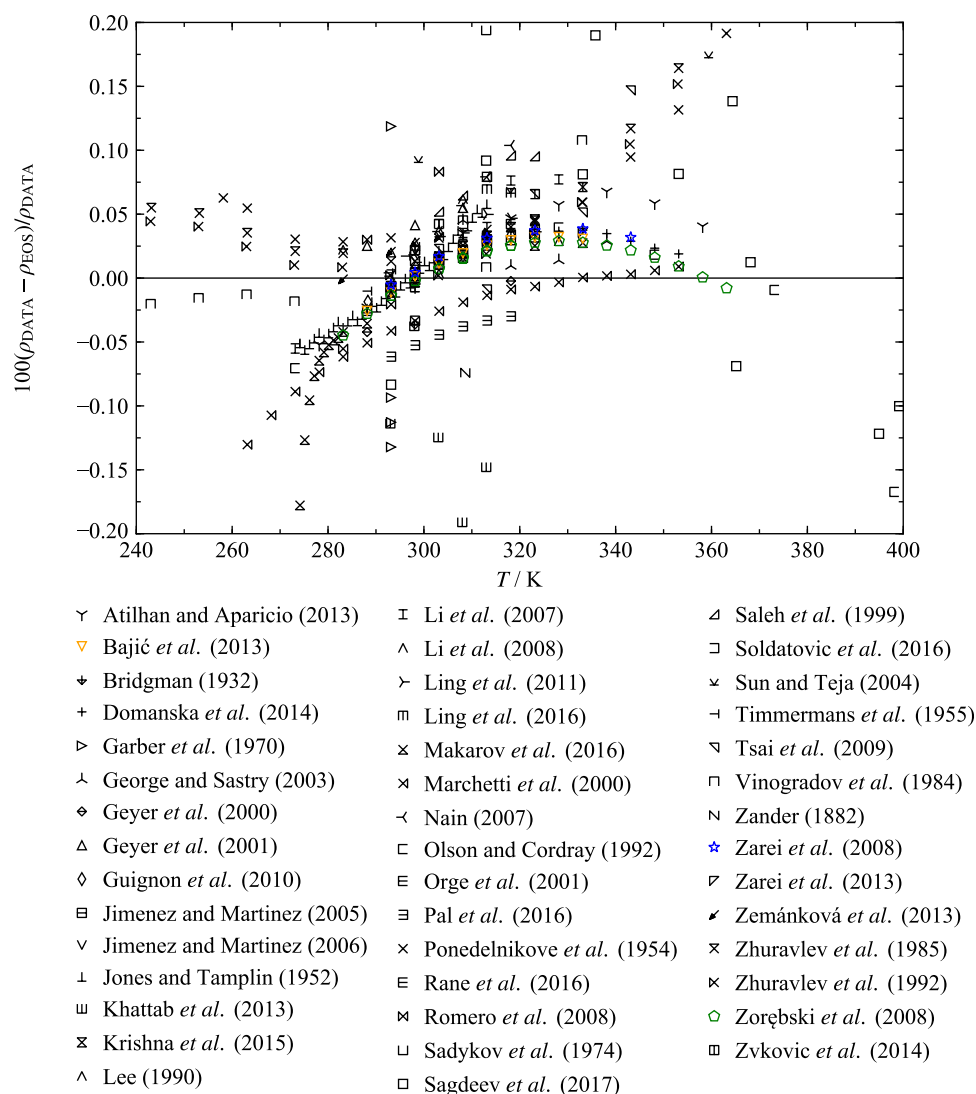


FIG. 8. Deviations of homogeneous liquid density data from the equation of state at atmospheric pressure as a function of temperature.

The vapor-pressure data cover a temperature range of 273–496 K. Most of them are limited to fairly small vapor pressures from roughly 3.4×10^{-6} MPa to 0.27 MPa. This has to be considered when assessing the percentage deviation of the data as shown in Fig. 9. Similar to the density measurements, there is a lack of data in the range of 200 K below the critical point due to the thermal decomposition of propylene glycol.

Nicolae and Oprea¹⁰⁴ and Fendu and Oprea⁹⁸ provided vapor-pressure measurements between 350 and 426 K. Both datasets were measured with the same static apparatus, consisting of an equilibrium cell that is connected to a U-shaped tube and heated by a thermostatic oil bath. Fendu and Oprea⁹⁸ measured vapor–liquid equilibrium data of propylene glycol mixtures and for the pure substances as well. In order to validate their experimental procedure, they refer to the data of Nicolae and Oprea¹⁰⁴ obtained for pure propylene glycol, which are in

very good agreement with the recent data of Fendu and Oprea.⁹⁸ However, with the exact same apparatus, high consistency is to be expected. For the given temperature range, both datasets contain corresponding vapor-pressure data between 0.8 and 25 kPa. The reported standard uncertainties of 0.012 and 0.034 kPa (0.028–0.29% for $k = 2$, respectively) are misleading because they are only related to the reproducibility of three repetitive measurements at each state point. Combined uncertainties are expected to be higher. Figure 9 shows that the data of Nicolae and Oprea¹⁰⁴ and Fendu and Oprea⁹⁸ deviate from the present equation of state by 2.9% and 2.7%, respectively.

In the vicinity of the normal boiling point, a cluster of single state points from 20 publications is available (cf. Table 12). Dean⁴² reported a normal-boiling-point temperature of 461.15 K, which deviates by -0.074 K (0.23%) from the calculated normal-boiling-point temperature in this work. Furthermore, the temperature of

TABLE 12. Summary of vapor–pressure (p_v) and saturated liquid density (ρ') data along with the temperature ranges and their AADs with respect to the equation of state

Author	Year	N	T (K)	AAD/%			
				LT ^a	MT ^a	HT ^a	Overall
p_v							
Chyliński <i>et al.</i> ⁹⁷	2004	8	393–424	3.8	4.2		4
Fendu and Oprea ⁹⁸	2014	16	350–426	1.9	0.43		1.4
Giles <i>et al.</i> ⁹⁹	1997	2	373–454	2.9	2.7		2.8
Horstmann <i>et al.</i> ¹⁰⁰	2001	2	338–349	26			26
Jones and Tamplin ⁶¹	1952	15	293–434	2.7	0.42		2.2
Kundu <i>et al.</i> ¹⁰¹	1970	9	278–319	3.5			3.5
Marsden <i>et al.</i> ¹⁰²	1954	10	318–462	11	0.78		7.2
Mathuni <i>et al.</i> ¹⁰³	2011	12	378–461	2.1	0.67		1
Nicolae and Oprea ¹⁰⁴	2014	15	350–421	1.9	0.48		1.6
Puck and Wise ¹⁰⁵	1946	5	298–353	11			11
Rane <i>et al.</i> ⁷⁴	2016	17	389–444	5.4	5.6		5.6
Riddick and Toops ¹⁰⁶	1955	7	298–462	4.8	0.78		2.5
Sokolov <i>et al.</i> ¹⁰⁷	1972	5	356–462	5.7	0.15		3.5
Steele <i>et al.</i> ⁴¹	2002	20	365–496	3.2	2.4		2.7
Stull ¹⁰⁸	1947	10	318–462	11	0.78		7.2
Verevkin ¹⁰⁹	2004	14	283–332	7.4			7.4
Verevkin <i>et al.</i> ¹¹⁰	2009	19	293–330	7.5			7.5
Wilding <i>et al.</i> ⁴⁵	1991	3	348–474	6.6	2.6		5.3
Wilson <i>et al.</i> ¹¹¹	1989	2	273–313	45			45
Xie and Chen ¹¹²	1993	14	358–460	35	12		20
Zhang <i>et al.</i> ¹¹³	2013	21	390–461	2.2	0.68		1
All authors with only one data point		20	459–463		1.9		1.9
ρ'							
Horstmann <i>et al.</i> ¹⁰⁰	2001	1	298.15	0.026			0.026
Steele <i>et al.</i> ⁴¹	2002	6	323–449	0.068	0.26		0.13
Wilding <i>et al.</i> ⁴⁵	1991	1	298.00	0.32			0.32
Zander ¹¹⁴	1882	9	288–451	4.8	18		11

^aLT: $T/T_c < 0.6$, MT: $0.6 \leq T/T_c \leq 0.98$, and HT: $T/T_c > 0.98$.

Marsden *et al.*¹⁰² at 461.35 K, which is highly referenced in the literature, agrees within +0.125 K (0.38%) with the equation.

One of the most comprehensive vapor–pressure datasets was obtained by Steele *et al.*⁴¹ The measurements were carried out in a twin ebulliometric apparatus covering a temperature range from 365 to 496 K. They claim rather small uncertainties between 0.003 kPa (0.015%) and 0.02 kPa (0.007%) at higher temperatures. However, the data significantly deviate from those of Nicolae and Oprea¹⁰⁴ and other researchers, e.g., Zhang *et al.*¹¹³ and Mathuni *et al.*¹⁰³ Therefore, they were not considered in the fitting procedure but are still reproduced within 3.8%.

The dataset of Kundu *et al.*¹⁰¹ contains measurements in the low-temperature region and yields correspondingly low vapor pressures from 2.7 to 90 Pa. These data agree with the measurements of Jones and Tamplin,⁶¹ and they connect appropriately to the data of Nicolae and Oprea¹⁰⁴ at higher temperatures. Therefore, these data were preferred over those of Verevkin,¹⁰⁹ which exhibit a contradictory trend. Percentage deviations of the data of Kundu *et al.*¹⁰¹ are up to 7%.

Due to the numerically small values of vapor pressures calculated with the present equation of state, percentage uncertainties are higher than for other fluids. They are estimated to be 5% ($k = 2$) between 290 and 500 K and are expected to increase at lower temperatures.

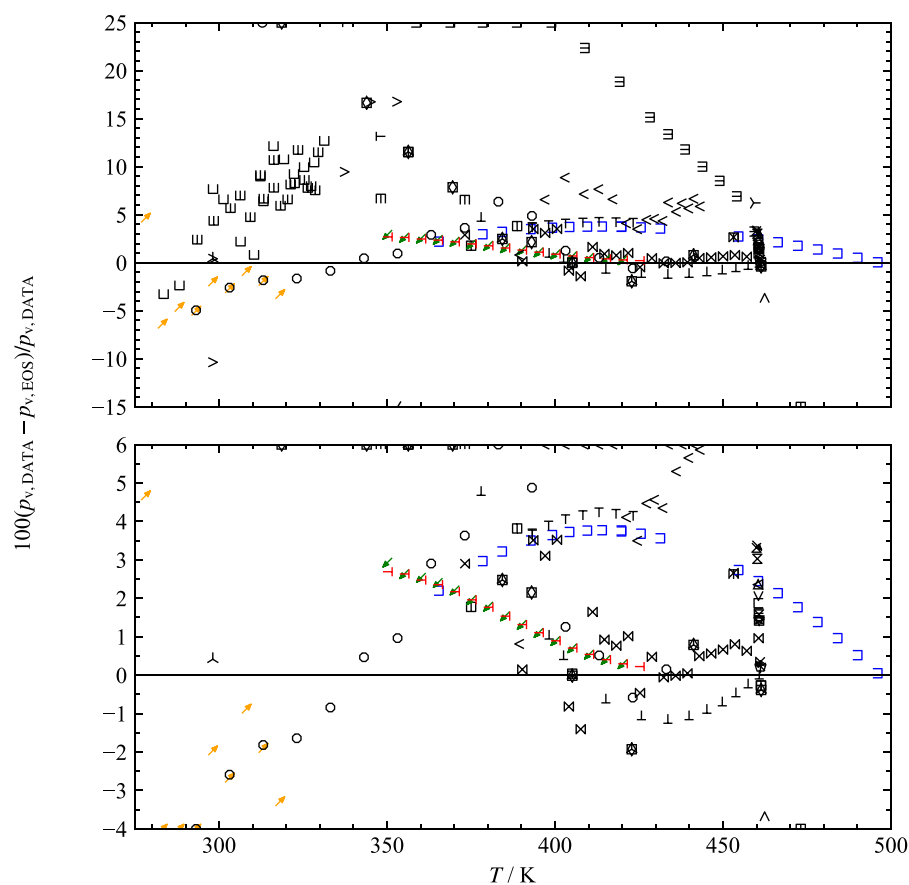
9.3. Comparisons of caloric properties

In comparison to the thermal properties, the caloric data are rather limited, including 172 speed-of-sound (Table 13) and 73 isobaric-heat-capacity (Table 14) data points.

The temperature and pressure ranges of all available speed-of-sound data are covered by the datasets of Dávila *et al.*¹⁶ and Zorębski *et al.*²⁷ The two sets together include measurements in a temperature range of 292–354 K with pressures up to 102 MPa. The data show excellent agreement at moderate pressures. Discrepancies can be observed at higher pressures ($p > 10$ MPa, cf. Fig. 10). To clarify this situation, new measurements were performed in this work, which perfectly agree with the measurements of Dávila *et al.*¹⁶

The data of Zorębski *et al.*²⁷ contain 45 state points in a very narrow temperature range of 292–314 K from ambient pressure up to 102 MPa. They claim an uncertainty of 1 m s^{-1} , which corresponds to a percentage deviation of 0.067% over the entire temperature range. Excluding the outlier at 15.2 MPa and 293 K, the dataset of Zorębski *et al.*²⁷ is well represented by the equation of state with deviations of less than 0.051%.

The measurements of Dávila *et al.*¹⁶ comprise 28 data points, from ambient pressure to 30.2 MPa in a temperature range of



⊥ Chyliński <i>et al.</i> (2004)	☆ Marcus (1998)	□ Sokolov <i>et al.</i> (1971)
⋄ Clendenning <i>et al.</i> (1950)	◇ Marsden (1954)	▣ Sokolov <i>et al.</i> (1972)
○ Dean (1999)	⊥ Mathuni <i>et al.</i> (2011)	▢ Steele <i>et al.</i> (2002)
➤ Fendu and Oprea (2014)	⋄ Mitchell and Tyrrell (1972)	□ Stull (1947)
△ Gallant (1968)	⋄ Musavirov <i>et al.</i> (1978)	▣ Subramanian <i>et al.</i> (1975)
× Garcia and Paz Andrade (1974)	⋄ Nageshwar <i>et al.</i> (1968)	⊥ Verevkin <i>et al.</i> (2009)
× Gardner <i>et al.</i> (1972)	➤ Nicolae and Oprea (2014)	▢ Verevkin (2004)
× Giles <i>et al.</i> (1997)	> Puck <i>et al.</i> (1946)	⊥ Wilding <i>et al.</i> (1991)
⋄ Haynes (2016)	< Rane <i>et al.</i> (2016)	○ Wilson <i>et al.</i> (1989)
⊥ Horstmann <i>et al.</i> (2001)	⋄ Riddick <i>et al.</i> (1955)	⊥ Xie and Chen (1993)
× Hu <i>et al.</i> (2015)	⋄ Riddick <i>et al.</i> (1986)	⊥ Yang <i>et al.</i> (2015)
○ Jones and Tamplin (1952)	⋄ Schierholtz <i>et al.</i> (1935)	⊥ Yaws (1999)
➤ Kundu <i>et al.</i> (1970)	⋄ Sevgili <i>et al.</i> (2008)	⊥ Zhang <i>et al.</i> (2013)
⋄ Mamedov <i>et al.</i> (2009)	⊥ Shi <i>et al.</i> (1999)	⊥ Zhong <i>et al.</i> (2014)

FIG. 9. Deviations of all available vapor-pressure data from the equation of state as a function of temperature. The bottom panel depicts the same data with a higher resolution of the y axis.

303–354 K. The experimental uncertainty is stated to be 0.02%. Both measurements were conducted with the ultrasonic pulse-echo-overlap method as already explained in detail in Sec. 3.1. However, Dávila *et al.*¹⁶ used a sample with higher purity (99.87 mol %) than

that used by Zorębski *et al.*²⁷ (99 mol %) and therefore reported a smaller experimental uncertainty. Except for one state point at atmospheric pressure, all data are represented within the experimental uncertainty. At ambient temperatures of 303 and 313 K, the data

TABLE 13. Summary of all liquid-phase speed-of-sound data along with the temperature and pressure ranges and their AADs with respect to the equation of state

Author	Year	<i>N</i>	<i>T</i> (K)	<i>p</i> (MPa)	AAD (%)
Dávila <i>et al.</i> ¹⁶	2016	28	303–354	<0.1–30.2	0.007
George and Sastry ⁵⁷	2003	5	298–339	0.101 325	0.91
Grzybkowski and Warmińska ¹¹⁵	2016	1	298.15	0.1	0.032
Kishimoto and Nomoto ¹¹⁶	1954	6	288–314	0.101 325	0.12
Krishna <i>et al.</i> ⁶³	2015	6	298–324	0.101 325	0.15
Krivokhizha and Fabelinskiĭ ¹¹⁷	1966	10	246–294	0.101 325	4.9
Kushare <i>et al.</i> ¹¹⁸	2008	1	298.15	0.101 325	0.15
Latha <i>et al.</i> ¹¹⁹	2015	4	303–319	0.101 325	0.12
Marks ¹²⁰	1967	3	273–354	0.101 325	0.14
Nain ¹²¹	2008	6	293–319	0.101 325	0.52
Pal <i>et al.</i> ⁷²	2016	6	293–319	0.1	0.11
Palani and Geetha ¹²²	2009	3	303–313	0.101 325	0.24
Ponedelnikova and Tarasova ⁷³	1954	12	258–364	0.101 325	0.33
Sastry and Patel ¹²³	2003	2	298–309	0.101 325	1.5
This work	2021	24	293–354	0.5–20.0	0.009
Tsierkezos and Palaiologou ¹²⁴	2009	1	298.15	0.101 325	0.018
Zorębski <i>et al.</i> ²⁷	2008	45	292–314	0.1–102	0.022

TABLE 14. Summary of all isobaric-heat-capacity data along with the temperature range and their overall AADs with respect to the equation of state

Author	Year	<i>N</i>	<i>T</i> (K)	<i>p</i> (MPa)	AAD (%)
Dean ⁴²	1999	1	298.15	0.101 325	0.66
Li <i>et al.</i> ¹²⁶	2009	6	303–354	0.101 325	0.66
Parks and Huffman ¹²⁷	1927	4	274–277	0.101 325	0.61
Pietrzak and Łudzik ¹²⁸	2015	1	298.15	0.1	1.1
Riddick <i>et al.</i> ¹²⁹	1986	1	293.14	0.101 325	0.75
Zemánková <i>et al.</i> ⁸⁶	2013	5	283–314	0.101 325	0.93
Zorębski <i>et al.</i> ²⁷	2008	55	293–314	0.1–100	0.29

points of Dávila *et al.*¹⁶ and Zorębski *et al.*²⁷ match within 0.009 percentage points (cf. Fig. 11), which shows the consistency of the datasets in that specific region. However, Fig. 10 shows that at pressures above ~10 MPa, the two datasets differ from each other and the data of Zorębski *et al.*²⁷ slightly scatter. Therefore, measurements were carried out in this work to clarify this situation. For details, see Sec. 3. These measurements prove the data of Dávila *et al.*¹⁶ to be more accurate. Therefore, our measurements were prioritized during the fitting procedure and are reproduced within 0.021%, which is well within the experimental uncertainty.

Figure 11 illustrates percentage deviations of experimental atmospheric speed-of-sound data from the present equation of state. The dataset of Zorębski *et al.*²⁷ is in very good agreement with two independent, single-point measurements of Grzybkowski and Warmińska¹¹⁵ and Tsierkezos and Palaiologou¹²⁴ at 298.15 K. Grzybkowski and Warmińska¹¹⁵ claimed an uncertainty of 0.15 m s⁻¹, which corresponds to a percentage deviation of 0.01%. It was measured with the pulse-echo method, with a sample of 99.5 mol % purity. The measurement of Tsierkezos and Palaiologou¹²⁴ was carried out with a similar purity but is associated with a higher

uncertainty (1 m s⁻¹) due to a different measurement technique. They obtained the speed of sound with an Anton Paar (type: DSA 48) sound analyzer. Usually, this technique has high precision but also requires complicated calibration procedures, which can cause considerable uncertainties according to Dzida *et al.*¹²⁵

Based on the data measured in this work and by Dávila *et al.*¹⁶ the uncertainties of speed-of-sound values calculated with the present equation of state are 0.03% (*k* = 2) between 290 and 360 K with a maximum pressure of 30 MPa. At higher pressures up to 100 MPa, uncertainties are estimated to be 0.07% in the same temperature range based on the data of Zorębski *et al.*²⁷

The available isobaric-heat-capacity data are listed in Table 14, and their deviations are shown in Fig. 12. All data were measured at atmospheric pressure and temperatures between 274 and 354 K, except for the dataset of Zorębski *et al.*²⁷ which provides data for the isobaric heat capacity at pressures up to 100 MPa.

The 55 data points of Zorębski *et al.*²⁷ were derived from speed-of-sound measurements at five isotherms covering a temperature range from 293 to 313 K. They used their speed-of-sound measurements to calculate the changes in isobaric heat capacity with

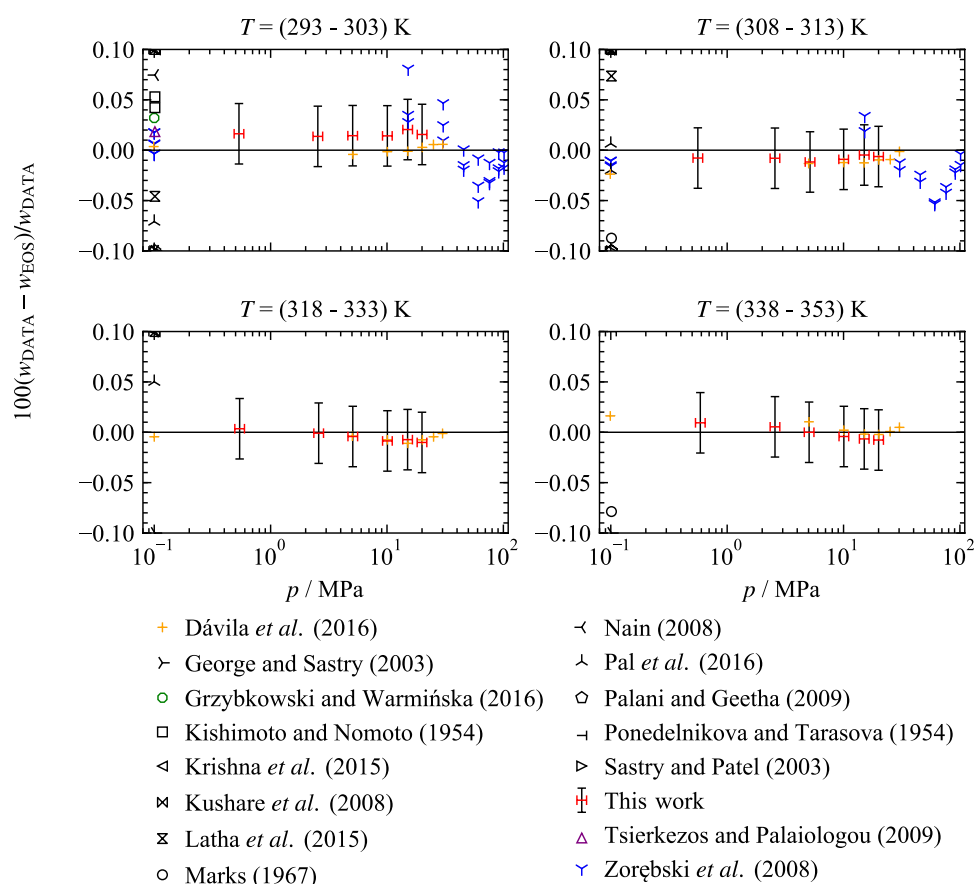


FIG. 10. Deviations of the available speed-of-sound data in the liquid phase from the equation of state in selected temperature ranges as a function of the logarithmic pressure along with the speed-of-sound data measured in this work.

varying pressure at constant temperature. As introduced by Sun *et al.*,⁹³ the actual calculations of the isobaric-heat-capacity data were performed with a polynomial, temperature-dependent fit based on smoothed values for the measured speed of sound, temperature, and pressure, as well as on reference values for the isobaric heat capacity at atmospheric pressure. Zorębski *et al.*²⁷ stated an uncertainty of 0.3% for the derived heat capacities of propylene glycol. At 303 and 313 K and atmospheric pressure, the corresponding data points of Zorębski *et al.*²⁷ and Li *et al.*¹²⁶ are in good agreement. The data of Zorębski *et al.*²⁷ deviate by less than 0.4% from the equation of state at atmospheric pressure, which increases up to 0.75% at the maximum pressure of 100 MPa. A more accurate representation of the data was not possible without deteriorating the speed-of-sound data of Zorębski *et al.*²⁷

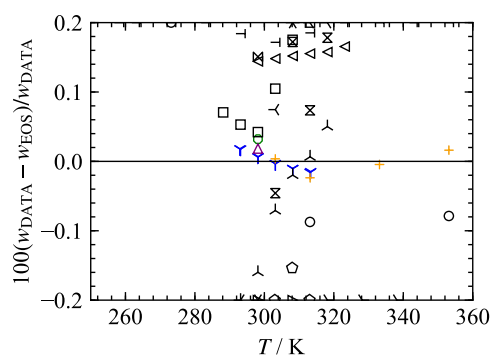
The dataset of Li *et al.*¹²⁶ contains isobaric-heat-capacity data in a temperature range from 303 to 354 K. They used a differential scanning calorimeter (DSC) to measure the isobaric heat capacity of propylene glycol as well as several mixtures of glycols, water, and salts. They claim an uncertainty of $0.015 \text{ kJ kg}^{-1} \text{ K}^{-1}$, which corresponds to an uncertainty of 0.5%–0.6%. All data obtained by Li *et al.*¹²⁶ are represented within 1.0% with the equation of state. Again, a better

representation of the data was not possible without degrading the speed-of-sound data.

Zemánková *et al.*⁸⁶ provided the third comprehensive dataset of isobaric heat capacity for propylene glycol. It covers a temperature range from 283 to 313 K at atmospheric pressure and was carried out with a Micro DSC III (Setaram, Caluire-et-Cuire, France) DSC and a 99.5 mass % pure probe. All data are represented within their estimated relative uncertainty of 0.5% and are in good agreement with the data reported by Dean⁴² and Riddick¹²⁹ at 298 and 293 K, respectively.

The dataset obtained by Parks and Huffman¹²⁷ contains 39 data points that are not entirely included in the analysis here since data are predominantly measured within the glassy state. The four liquid data points at 275–277 K are represented within less than 0.8% with the equation of state.

Since the heat-capacity data at atmospheric pressure scatter and even exhibit different trends (cf. Fig. 12), it is difficult to reliably state an uncertainty of values calculated with the present equation of state. Therefore, it is conservatively assessed to be 1.5% ($k = 2$) within a temperature range of 270–360 K. Uncertainties at elevated pressures might be 1% based on the data of Zorębski *et al.*²⁷ However, additional measurements are required to prove this statement.

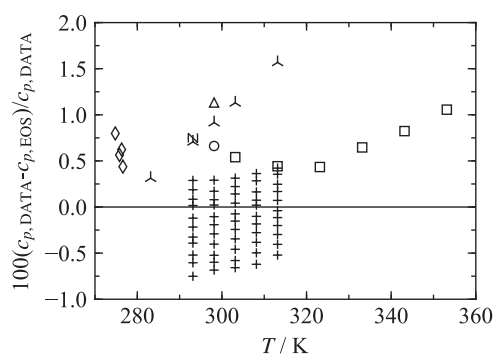


- + Dávila *et al.* (2016)
- ▷ George and Sastry (2003)
- Grzybkowski and Warمیńska (2016)
- Kishimoto and Nomoto (1954)
- ◁ Krishna *et al.* (2015)
- ✕ Kushare *et al.* (2008)
- ⊗ Latha *et al.* (2015)
- Marks (1967)
- ◁ Nain (2008)
- ♠ Pal *et al.* (2016)
- Palani and Geetha (2009)
- ◁ Ponedelnikova *et al.* (1954)
- ▷ Sastry and Valand (1998)
- △ Tsierkezos *et al.* (2009)
- ♠ Zorębski *et al.* (2008)

FIG. 11. Deviations of the available speed-of-sound data in the liquid phase from the equation of state at atmospheric pressure as a function of temperature.

10. Extrapolation and Physical Behavior

In addition to the precise representation of the experimental data, the extrapolation behavior must also be considered when assessing the quality of the equation of state. To ensure the physically correct behavior of the equation in fluid state regions at either very high or low temperatures and pressures and close to the critical point, a smooth and steady course of constant properties in those regions is very important. In the following analysis, the behavior of various thermal and caloric properties of propylene glycol is investigated. The fluid regions with strong associative behavior are expected to show deviating shapes of constant property lines, comparable to those of other strongly associating fluids, e.g., heavy water.¹³⁰ These peculiarities are predominantly observed in the consideration of caloric properties at low temperatures. Reasonable extrapolation behavior over a wide fluid range is of particular importance for propylene glycol. The relatively narrow region covered by experimental data can be extended in order to maintain a wider range of accessible fluid states. This is important when considering propylene glycol, e.g., as a hydrate inhibitor in mixture models. Mixture models are often evaluated in regions outside of the range of validity of the pure compounds. For asymmetric mixtures, such as propylene glycol and carbon dioxide, correct extrapolation behavior of the pure-fluid equation of state is mandatory.



- Dean (1999)
- Li *et al.* (2009)
- ◇ Parks and Huffman (1927)
- △ Pietrzak and Łudzik (2015)
- ⊗ Riddick *et al.* (1986)
- ♠ Zemánková *et al.* (2013)
- + Zorębski *et al.* (2008)

FIG. 12. Deviations of all available liquid-phase isobaric-heat-capacity data from the equation of state as a function of temperature.

The shapes of the “ideal curves” (cf. Ref. 131) are fundamental to evaluate the extrapolation behavior of an equation of state. Each ideal curve is usually defined in terms of derivatives of the compressibility factor with respect to temperature and density. The shapes of these ideal curves should be devoid of any bumps or discontinuities. The ideal curves calculated from the equation of state of this work show reasonable behavior over the entire temperature and pressure range. As illustrated in Fig. 13, the coverage of underlying measurements compared to other fluids (e.g., CO₂) is quite narrow for propylene glycol, and extrapolating outside this region requires that the ideal curves meet all criteria.

Figure 14 depicts two other important criteria for the thermal properties. In the top panel, a double-logarithmic pressure–density diagram with selected isotherms up to 10⁶ K is shown. At high pressures, isotherms should merge with increasing temperature without crossing each other. In the bottom panel, a temperature–density plot with selected isobars is presented. It shows a straight rectilinear diameter $\rho_{RD} = (\rho' + \rho'')/2$ up to the critical point and a distinct saddle point of the critical isobar at this point.

Another criterion for assessing the extrapolation behavior of the equation of state can be derived from the shape of the second (*B*), third (*C*), and fourth (*D*) virial coefficients. Starting at low temperatures and negative infinity, all three virial coefficients have a positive slope and negative curvature until they cross the zero line. They exhibit a maximum and approach zero without becoming negative again. The maxima of the third and fourth virial coefficients are expected to be around the critical temperature for simple fluids, such as noble gases; cf. Ref. 132. However, this might not be true for associating fluids, such as propylene glycol, water,²⁶ or heavy water.¹³⁰ The maximum values are slightly shifted here. The theoretical behavior of the fourth virial coefficient is defined by a second, smaller maximum at higher temperatures as shown by Thol *et al.*,¹³² which is fulfilled by the equation of state (cf. Fig. 15).

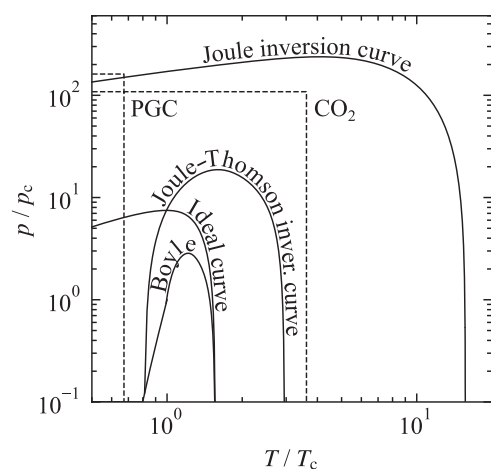


FIG. 13. Ideal curves for the equation of state for propylene glycol (PGC) in terms of the reduced temperature T/T_c and pressure p/p_c : vapor-pressure curve (p_v), Boyle curve, Joule–Thomson inversion curve, Joule inversion curve, and ideal curve. The dashed lines mark the regions covered by the experimental data for PGC and CO_2 .

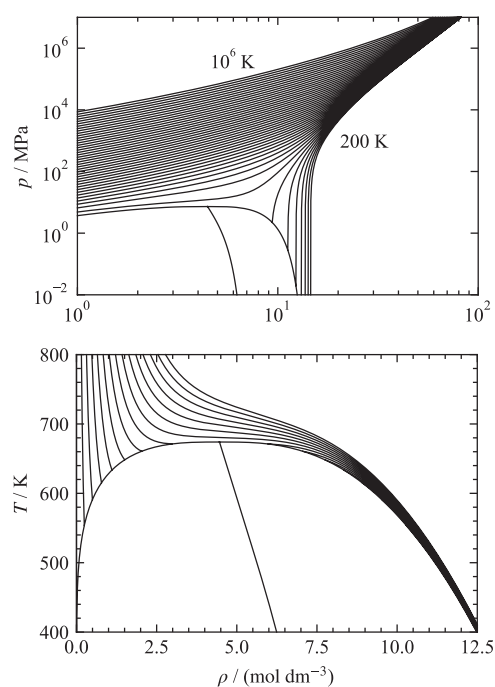


FIG. 14. p, ρ -diagram along isotherms up to 10^6 K (top). T, ρ -diagram showing the phase boundaries, the rectilinear diameter, and the critical isobar (bottom).

In the vicinity of the critical region, analytical equations show limitations for the calculation of thermal and caloric properties due to the mathematical structure. Moreover, measurements in this region are associated with high uncertainties, if available at all. According to Span,²⁹ the theoretical behavior of caloric properties close to and at the critical point is related to the pressure derivatives. The derivative

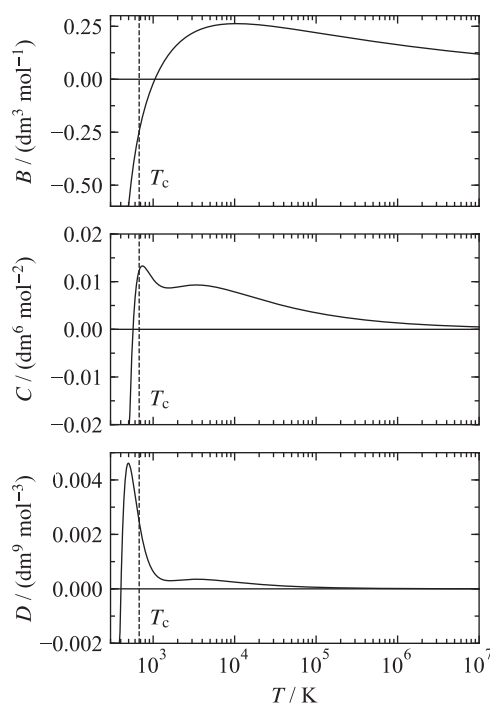


FIG. 15. Second (B), third (C), and fourth (D) virial coefficients. The dashed lines indicate the critical temperature.

$(\partial p/\partial \rho)_T$ becomes zero and $(\partial p/\partial T)_\rho$ reaches a finite value at the critical point, which yields, for example, a diverging isobaric heat capacity. However, zero sound speed and infinite isochoric heat capacity at the critical point cannot be obtained with the analytical equations, as currently used in all equation of state developments due to the mathematical structure. This would require the use of non-analytical terms such as those applied to the equations of state of carbon dioxide¹³³ and water,²⁶ which is not possible here due to the restricted database. Nonetheless, the equation should exhibit distinct minima/maxima at the critical point. The present equation of state includes two GBS terms to approach the desired behavior of the speed of sound and the residual isochoric heat capacity (see Figs. 16 and 17) in the critical region.

Figure 16 shows the speed of sound as a function of temperature along selected isobars. As expected, the liquid and vapor saturation curves merge in a distinct minimum. The three most comprehensive datasets for this property of Zorebski *et al.*,²⁷ Dávila *et al.*,¹⁶ and our results, covering isobars up to 100 MPa in the liquid phase, are included in the figure. Although these data cover only a small temperature and pressure range in the liquid phase, the equation shows a satisfactory course of the sound speed in the entire fluid region.

The residual isochoric heat capacity is closely related to the speed of sound. Accompanied by the distinct minimum of sound speed, the saturated liquid and vapor curves of the residual isochoric heat capacity merge in a distinct maximum at the critical point. In the vicinity of the critical point, the steep increasing saturation lines should cross each other and meet at the critical point, which is fulfilled by the equation of state (cf. Fig. 17). The conspicuous behavior between the

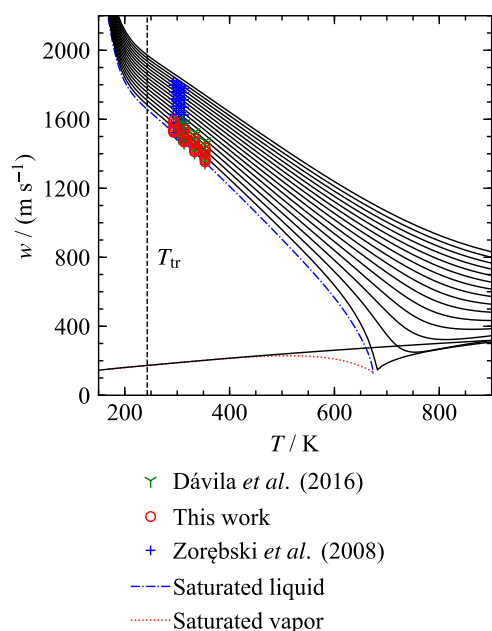


FIG. 16. Speed of sound along isobars up to 120 MPa (in steps of 8 MPa) as a function of temperature. The three most comprehensive datasets are plotted for a better assessment of the data situation. The dashed vertical line shows the lower temperature limit of the equation of state at the triple-point temperature.

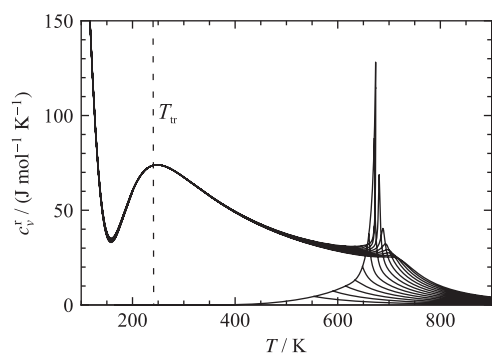


FIG. 17. Residual isochoric heat capacity along isobars up to 50 MPa (in steps of 5 MPa) as a function of temperature. The dashed line shows the lower temperature limit of the equation of state at the triple-point temperature.

glass-transition temperature of 169.15 K and the triple-point temperature of 242.8 K is due to a distinct change in the internal energy/enthalpy and, thus, in heat capacity in the transitional region between the glassy and the liquid state. This can also be observed for related properties such as the speed of sound (cf. Fig. 16).

Figure 18 shows the phase identification parameter¹³⁴ over a broad temperature range along various isobars for the present equation of state. Due to its high dependency on partial derivatives of pressure, volume, and temperature, the phase identification parameter is an important property when assessing the quality of the equation of state. Except for the association effects in the same

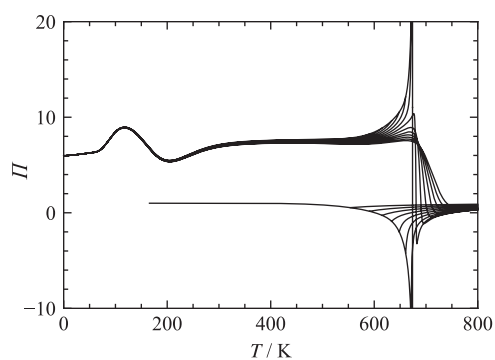


FIG. 18. Phase identification parameter as a function of temperature along selected isobars.

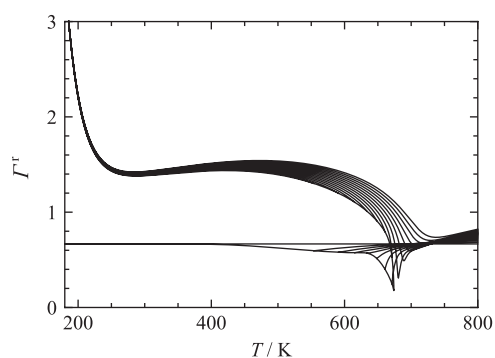


FIG. 19. Residual Grüneisen parameter as a function of temperature along selected isobars.

temperature range as for the isochoric heat capacity, the saturated liquid line should show all positive derivatives and a distinct maximum at the critical point, while the saturated vapor line should exhibit an opposing behavior and reach a minimum.

The Grüneisen parameter establishes the connection between thermal and caloric properties and is, thus, another important criterion in assessing the extrapolation behavior of the equation. Similar to the speed of sound, it should exhibit merging saturation lines with a distinct minimum at the critical point (cf. Fig. 19). At low temperatures, the association effect becomes obvious.

The analysis of these plots shows that the equation exhibits correct physical and extrapolation behavior and can thus be applied to mixture models.

11. Conclusion

A fundamental equation of state in terms of the Helmholtz energy with the independent variables temperature and density was developed for propylene glycol. Accurate speed-of-sound measurements were carried out with the pulse-echo technique between 293 and 354 K with a maximum pressure of 20 MPa in order to validate experimental data from the literature. The experimental uncertainty in the speed-of-sound measurements is estimated to be 0.03% ($k = 2$).

There were some particular challenges during the development of the equation of state, especially with the inadequate data situation. Propylene glycol exhibits quite strong association in the liquid phase, which particularly changes the behavior of properties in the lower temperature region. Furthermore, due to thermal decomposition, a broad temperature range has not been investigated experimentally and the critical point is not well known. There is no reliable information available on the isobaric heat capacity of the ideal gas so that the ideal part of the equation of state had to be adjusted to liquid speed-of-sound and heat-capacity data.

The equation can be used to calculate all thermodynamic properties between the triple-point temperature of 242.8 K and the maximum temperature of 680 K with pressures up to 350 MPa. Based on the experimental data, estimates of the uncertainties ($k = 2$) of the properties calculated with the equation of state are given in the corresponding parts of Sec. 9. The uncertainties of densities calculated with the present equation of state at atmospheric pressure are estimated to be 0.06% at temperatures between 270 and 380 K and increase up to 0.1% at lower temperatures. The uncertainty of calculated densities at elevated pressures is estimated to be 0.06% between 270 and 460 K with pressures up to 100 MPa. Uncertainties with respect to the calculated vapor pressures are 5% between 290 and 500 K and are expected to increase at lower temperatures. The uncertainties of liquid-phase speeds of sound calculated with the present equation of state are 0.03% between 290 and 360 K with a maximum pressure of 30 MPa. At higher pressures up to 100 MPa, uncertainties are estimated to be 0.07%. The calculated isobaric-heat-capacity data are assessed to be uncertain by 1.5% within a temperature range of 270–360 K at atmospheric pressure, whereas it is 1% at elevated pressures.

Since propylene glycol is a component in various mixture applications, special attention was given to reliable physical behavior of the equation in regions where no experimental data are available.

12. Supplementary Material

In the [supplementary material](#), a fluid file for application in the software packages TREND¹³⁵ and REFPROP¹³⁶ is provided (PROPYLENEGLYCOL.FLD). Furthermore, a stand-alone Python script is available for calculation of common thermodynamic properties with the present equation of state for propylene glycol (propyleneglycol.py). Additional Python files for use in CoolProp¹³⁷ are also provided (PropyleneGlycol.json, test_CoolProp_PG.py).

Acknowledgment

The authors thank Dr. Ian H. Bell for providing the Python script available in the [supplementary material](#).

Data Availability

The data that support the findings of this study are available within the article and its [supplementary material](#).

13. References

¹B. A. Steff and K. F. George, “Antifreezes and deicing fluids,” in *Kirk–Othmer Encyclopedia of Chemical Technology*, edited by R. E. Kirk and D. F. Othmer (John Wiley & Sons, New York, NY, 2000), pp. 1–21.

- ²A. Chapoy, R. W. Burgass, and B. Tohidi Kalorazi, “Hydrate inhibition in propylene glycol and glycerol systems,” paper presented at 8th International Conference on Gas Hydrates, Beijing, China, 2014.
- ³J. Gernert and R. Span, *J. Chem. Thermodyn.* **93**, 274 (2016).
- ⁴R. Feistel and W. Wagner, *J. Phys. Chem. Ref. Data* **35**, 1021 (2006).
- ⁵A. Jäger and R. Span, *J. Chem. Eng. Data* **57**, 590 (2012).
- ⁶J. P. M. Trusler, *J. Phys. Chem. Ref. Data* **40**, 043105 (2011).
- ⁷V. Vinš, A. Jäger, R. Span, and J. Hrubý, *Fluid Phase Equilib.* **427**, 268 (2016).
- ⁸V. Vinš, A. Jäger, J. Hrubý, and R. Span, *Fluid Phase Equilib.* **435**, 104 (2017).
- ⁹A. Jäger, V. Vinš, R. Span, and J. Hrubý, *Fluid Phase Equilib.* **429**, 55 (2016).
- ¹⁰J. A. Ruddick, *Toxicol. Appl. Pharmacol.* **21**, 102 (1971).
- ¹¹P. Boutron and A. Kaufmann, *Cryobiology* **16**, 557 (1979).
- ¹²N. H. Rhys, R. J. Gillams, L. E. Collins, S. K. Callar, M. J. Lawrence, and S. E. McLain, *J. Chem. Phys.* **145**, 224504 (2016).
- ¹³W. L. Howard, *J. Chem. Eng. Data* **14**, 129 (1969).
- ¹⁴M. E. Wieser and M. Berglund, *Pure Appl. Chem.* **81**, 2131 (2009).
- ¹⁵E. Tiesinga, P. J. Mohr, D. B. Newell, and B. N. Taylor, The 2018 CODATA Recommended Values of the Fundamental Physical Constants (Web Version 8.1). Database developed by J. Baker, M. Douma, S. Kotochigova, National Institute of Standards and Technology, Gaithersburg, 2020, available at <http://physics.nist.gov/constants>.
- ¹⁶M. J. Dávila, H. Gedanitz, and R. Span, *J. Chem. Thermodyn.* **101**, 199 (2016).
- ¹⁷H. Gedanitz, M. J. Dávila, E. Baumhögger, and R. Span, *J. Chem. Thermodyn.* **42**, 478 (2010).
- ¹⁸K. Meier and S. Kabelac, *Rev. Sci. Instrum.* **77**, 123903 (2006).
- ¹⁹R. Wegge, Thermodynamic Properties of the (Argon + Carbon Dioxide) System: Instrument Development and Measurements of Density and Speed of Sound, Ruhr-Universität Bochum, 2016.
- ²⁰R. Wegge, M. Richter, and R. Span, *J. Chem. Eng. Data* **60**, 1345 (2015).
- ²¹F. H. Dubberke, E. Baumhögger, and J. Vrabec, *Rev. Sci. Instrum.* **86**, 054903 (2015).
- ²²G. R. Harris, *J. Acoust. Soc. Am.* **70**, 186 (1981).
- ²³H. Gedanitz, Schallgeschwindigkeits- und Dichtemessungen in Fluiden, Ruhr-Universität Bochum, 2010.
- ²⁴V. A. Del Grosso and C. W. Mader, *J. Acoust. Soc. Am.* **52**, 1442 (1972).
- ²⁵K. Fujii and R. Masui, *J. Acoust. Soc. Am.* **93**, 276 (1993).
- ²⁶W. Wagner and A. Pruß, *J. Phys. Chem. Ref. Data* **31**, 387 (2002).
- ²⁷E. Zorębski, M. Dzida, and M. Piotrowska, *J. Chem. Eng. Data* **53**, 136 (2008).
- ²⁸K. Lucas, *Applied Statistical Thermodynamics* (Springer, Berlin, 1991).
- ²⁹R. Span, *Multiparameter Equations of State: An Accurate Source of Thermodynamic Property Data* (Springer, Berlin, 2000).
- ³⁰L. Haar, J. S. Gallagher, and G. S. Kell, “A thermodynamic surface of water: The formulation and computer programs,” in *Proceedings of the 8th Symposium on Thermophysical Properties*, edited by J. V. Sengers (American Society of Mechanical Engineers (ASME), New York, 1982), pp. 298–302.
- ³¹U. Setzmann and W. Wagner, *J. Phys. Chem. Ref. Data* **20**, 1061 (1991).
- ³²K. Gao and E. W. Lemmon (private communication to T. Eisenbach, 2020).
- ³³E. Diaz, M. E. Sad, and E. Iglesia, *ChemSusChem* **3**, 1063 (2010).
- ³⁴D. M. VonNiederhausern, G. M. Wilson, and N. F. Giles, *J. Chem. Eng. Data* **45**, 157 (2000).
- ³⁵A. Kazakov, C. D. Muzny, V. Diky, R. D. Chirico, and M. Frenkel, *Fluid Phase Equilib.* **298**, 131 (2010).
- ³⁶W. H. Carande, A. Kazakov, C. Muzny, and M. Frenkel, *J. Chem. Eng. Data* **60**, 1377 (2015).
- ³⁷D. M. VonNiederhausern, L. C. Wilson, N. F. Giles, and G. M. Wilson, *J. Chem. Eng. Data* **45**, 154 (2000).
- ³⁸K. G. Joback and R. C. Reid, *Chem. Eng. Commun.* **57**, 233 (1987).
- ³⁹B. E. Poling, J. M. Prausnitz, and J. P. O’Connell, *The Properties of Gases and Liquids*, 5th ed. (McGraw-Hill, Inc., New York, 2001).
- ⁴⁰C. C. Sampson, X. Yang, J. Xu, and M. Richter, *J. Chem. Thermodyn.* **131**, 206 (2019).
- ⁴¹W. V. Steele, R. D. Chirico, S. E. Knipmeyer, and A. Nguyen, *J. Chem. Eng. Data* **47**, 689 (2002).

- ⁴²J. A. Dean, *Lange's Handbook of Chemistry* (McGraw-Hill, Inc., New York, 1999).
- ⁴³C. L. Yaws, *Chemical Properties Handbook: Physical, Thermodynamic, Environmental, Transport, Safety, and Health Related Properties for Organic and Inorganic Chemicals* (McGraw-Hill, Inc., New York, 1999).
- ⁴⁴R. W. Gallant, *Physical Properties of Hydrocarbons* (Gulf Publishing Company, Texas, 1968).
- ⁴⁵W. V. Wilding, L. C. Wilson, and G. M. Wilson, *AIChE Data Ser.* **1**, 6 (1991).
- ⁴⁶VDI-Gesellschaft Verfahrenstechnik und Chemieingenieurwesen (GVC), *VDI Wärmeatlas* (Springer, Berlin, Heidelberg, 2013).
- ⁴⁷V. Diky, C. D. Muzny, A. Y. Smolyanitsky, A. Bazyleva, R. D. Chirico, J. W. Magee, Y. Paulechka, A. F. Kazakov, S. A. Townsend, E. W. Lemmon, M. Frenkel, and K. Kroenlein, ThermoData Engine (TDE) Version 10.2 (Pure Compounds, Binary Mixtures, Ternary Mixtures, and Chemical Reactions): NIST Standard Reference Database 103b, National Institute of Standards and Technology, Gaithersburg, 2019.
- ⁴⁸V. Diky, R. D. Chirico, C. D. Muzny, A. F. Kazakov, K. Kroenlein, J. W. Magee, I. Abdulgatov, and M. Frenkel, *J. Chem. Inf. Model.* **53**, 3418 (2013).
- ⁴⁹E. W. Lemmon and R. Span, *J. Chem. Eng. Data* **60**, 3745 (2015).
- ⁵⁰M. Thol, G. Rutkai, A. Köster, F. H. Dubberke, T. Windmann, R. Span, and J. Vrabec, *J. Chem. Eng. Data* **61**, 2580 (2016).
- ⁵¹B. Guignon, C. Aparicio, and P. D. Sanz, *J. Chem. Eng. Data* **55**, 3017 (2010).
- ⁵²P. W. Bridgman, *Proc. Am. Acad. Arts Sci.* **67**, 1 (1932).
- ⁵³M. Atilhan and S. Aparicio, *J. Chem. Thermodyn.* **57**, 137 (2013).
- ⁵⁴D. M. Bajić, G. R. Ivaniš, Z. P. Visak, E. M. Zivković, S. P. Šerbanović, and M. L. Kijevčanin, *J. Chem. Thermodyn.* **57**, 510 (2013).
- ⁵⁵U. Domańska, P. Papis, J. Szydłowski, M. Królikowska, and M. Królikowski, *J. Phys. Chem. B* **118**, 12692 (2014).
- ⁵⁶Y. N. Garber, L. F. Komarova, L. I. Aleinikova, and L. S. Fomina, *Zh. Prikl. Khim.* **43**, 2658 (1970).
- ⁵⁷J. George and N. V. Sastry, *J. Chem. Eng. Data* **48**, 1529 (2003).
- ⁵⁸H. Geyer, P. Ulbig, and M. Görnert, *J. Chem. Thermodyn.* **32**, 1585 (2000).
- ⁵⁹H. Geyer, P. Ulbig, M. Görnert, and A. Susanto, *J. Chem. Thermodyn.* **33**, 987 (2001).
- ⁶⁰J. Jiménez and F. Martínez, *Rev. Colomb. Cienc. Quím.-Farm.* **34**, 46 (2005).
- ⁶¹W. S. Jones and W. S. Tamplin, "Physical properties of propylene glycol in glycols," in *American Chemical Society Monograph*, edited by G. O. Curme, Jr. (Reinhold Publishing Corporation, New York, NY, 1952) Chap. 9, Vol. 114, pp. 210-240.
- ⁶²I. S. Khattab, F. Bandarkar, M. Khoubnasabjafari, and A. Jouyban, *Arabian J. Chem.* **10**, 71 (2013).
- ⁶³T. S. Krishna, M. Gowri Sankar, K. R. Thomas, S. Govardhan Rao, and B. Munibhadrayya, *J. Mol. Liq.* **206**, 350 (2015).
- ⁶⁴Q.-S. Li, M.-G. Su, and S. Wang, *J. Chem. Eng. Data* **52**, 1141 (2007).
- ⁶⁵Q.-S. Li, Y.-M. Tian, and S. Wang, *J. Chem. Eng. Data* **53**, 271 (2008).
- ⁶⁶J.-L. Ling, F. Cao, M. Xu, and L. Yu, *J. Chem. Ind. Eng. China* **62**, 1191 (2011).
- ⁶⁷J.-L. Ling, L. Li, and J.-L. Yang, *J. Chem. Eng. Chin. Univ.* **30**, 268 (2016).
- ⁶⁸D. M. Makarov, G. I. Egorov, and A. M. Kolker, *J. Mol. Liq.* **222**, 656 (2016).
- ⁶⁹A. Marchetti, G. Pályi, L. Tassi, A. Ulrici, and C. Zucchi, *J. Mol. Liq.* **88**, 183 (2000).
- ⁷⁰A. K. Nain, *J. Chem. Thermodyn.* **39**, 462 (2007).
- ⁷¹J. D. Olson and D. R. Cordray, *Fluid Phase Equilib.* **76**, 213 (1992).
- ⁷²A. Pal, M. Saini, and B. Kumar, *Fluid Phase Equilib.* **411**, 66 (2016).
- ⁷³E. G. Ponedelnikova and V. V. Tarasova, *Dokl. Akad. Nauk SSSR* **96**, 1191 (1954).
- ⁷⁴N. V. Rane, A. Kumari, J. Soujanya, and B. Satyavathi, *J. Chem. Thermodyn.* **97**, 142 (2016).
- ⁷⁵C. M. Romero, M. S. Páez, and D. Pérez, *J. Chem. Thermodyn.* **40**, 1645 (2008).
- ⁷⁶A. K. Sadykov, D. I. Sagdeev, V. P. Brykov, and G. K. Mukhamedzyanov, *Tr. Kazan. Khim.-Tekhnol. Inst.* **53**, 98 (1974).
- ⁷⁷D. I. Sagdeev, M. G. Fomina, and I. M. Abdulgatov, *Fluid Phase Equilib.* **450**, 99 (2017).
- ⁷⁸M. A. Saleh, S. Begum, S. K. Begum, and B. A. Begum, *Phys. Chem. Liq.* **37**, 785 (1999).
- ⁷⁹D. A. Soldatović, J. M. Vuksanović, I. R. Radović, and M. L. Kijevčanin, *J. Chem. Thermodyn.* **102**, 105 (2016).
- ⁸⁰T. Sun and A. S. Teja, *J. Chem. Eng. Data* **49**, 1311 (2004).
- ⁸¹J. Timmermans and Hennaut-Roland, *J. Chim. Phys.* **52**, 223 (1955).
- ⁸²C.-Y. Tsai, A. N. Soriano, and M.-H. Li, *J. Chem. Thermodyn.* **41**, 623 (2009).
- ⁸³A. N. Vinogradov and M. I. Shakhparonov, *Viniti, Code 1479-78*, 1, 1984.
- ⁸⁴H. A. Zarei, S. Asadi, and H. Iloukhani, *J. Mol. Liq.* **141**, 25 (2008).
- ⁸⁵H. Zarei, S. A. Golroudbari, and M. Behroozi, *J. Mol. Liq.* **187**, 260 (2013).
- ⁸⁶K. Zemánková, J. Troncoso, and L. Romani, *Fluid Phase Equilib.* **356**, 1 (2013).
- ⁸⁷V. I. Zhuravlev, *Zh. Fiz. Khim.* **66**, 225 (1992).
- ⁸⁸V. I. Zhuravlev, V. A. Durov, T. M. Usacheva, and M. I. Shakhparonov, *Zh. Obshch. Khim.* **55**, 992 (1985).
- ⁸⁹E. M. Zivković, D. M. Bajić, I. R. Radović, S. P. Šerbanović, and M. L. Kijevčanin, *Fluid Phase Equilib.* **373**, 1 (2014).
- ⁹⁰Y. Kayukawa, M. Hasumoto, and K. Watanabe, *Rev. Sci. Instrum.* **74**, 4134 (2003).
- ⁹¹S. L. Outcalt and M. O. McLinden, *Ind. Eng. Chem. Res.* **46**, 8264 (2007).
- ⁹²E. F. May, W. J. Tay, M. Nania, A. Aleji, S. Al-Ghafri, and J. P. M. Trusler, *Rev. Sci. Instrum.* **85**, 095111 (2014).
- ⁹³T. F. Sun, C. A. Ten Seldam, P. J. Kortbeek, N. J. Trappeniers, and S. N. Biswas, *Phys. Chem. Liq.* **18**, 107 (1988).
- ⁹⁴J. P. M. Trusler and E. W. Lemmon, *J. Chem. Thermodyn.* **109**, 61 (2017).
- ⁹⁵W. Wagner and M. Thol, *J. Phys. Chem. Ref. Data* **44**, 043102 (2015).
- ⁹⁶B. Orge, B. E. de Cominges, G. Marino, M. Iglesias, and J. Tojo, *Phys. Chem. Liq.* **39**, 99 (2001).
- ⁹⁷K. Chyliński, Z. Fraś, and S. K. Malanowski, *J. Chem. Eng. Data* **49**, 18 (2004).
- ⁹⁸E. M. Fendu and F. Oprea, *Fluid Phase Equilib.* **382**, 244 (2014).
- ⁹⁹N. F. Giles, L. C. Wilson, G. M. Wilson, and W. V. Wilding, *J. Chem. Eng. Data* **42**, 1067 (1997).
- ¹⁰⁰S. Horstmann, H. Gardeler, K. Fischer, F. Köster, and J. Gmehling, *J. Chem. Eng. Data* **46**, 337 (2001).
- ¹⁰¹K. K. Kundu, P. K. Chattopadhyay, D. Jana, and M. N. Das, *J. Chem. Eng. Data* **15**, 209 (1970).
- ¹⁰²C. Marsden, *Solvents and Allied Substances Manual* (Cleaver-Hume Press LTD, London, 1954).
- ¹⁰³T. Mathuni, J.-I. Kim, and S.-J. Park, *J. Chem. Eng. Data* **56**, 89 (2011).
- ¹⁰⁴M. Nicolae and F. Oprea, *Fluid Phase Equilib.* **370**, 34 (2014).
- ¹⁰⁵T. T. Puck and H. Wise, *J. Phys. Chem.* **50**, 329 (1946).
- ¹⁰⁶J. A. Riddick and E. E. Toops, *Organic Solvents: Physical Properties and Methods of Purification* (Interscience Publishers Inc., New York, NY, 1955).
- ¹⁰⁷N. M. Sokolov, L. N. Tsygankova, M. I. Shtrom, and N. M. Zhavoronkov, *Sov. Chem. Ind.* **48**, 427 (1972).
- ¹⁰⁸D. R. Stull, *Ind. Eng. Chem.* **39**, 517 (1947).
- ¹⁰⁹S. P. Verevkin, *Fluid Phase Equilib.* **224**, 23 (2004).
- ¹¹⁰S. P. Verevkin, V. N. Emel'yanenko, and G. Nell, *J. Chem. Thermodyn.* **41**, 1125 (2009).
- ¹¹¹L. C. Wilson, W. V. Wilding, and G. M. Wilson, *AIChE Symp. Ser.* **85**, 25 (1989).
- ¹¹²R. Xie and C. Chen, *J. Chem. Eng. Chin. Univ.* **7**, 267 (1993).
- ¹¹³L. Zhang, W. Wu, Y. Sun, L. Li, B. Jiang, X. Li, N. Yang, and H. Ding, *J. Chem. Eng. Data* **58**, 1308 (2013).
- ¹¹⁴A. Zander, *Justus Liebigs Ann. Chem.* **214**, 138 (1882).
- ¹¹⁵W. Grzybowski and D. Warمیńska, *J. Chem. Eng. Data* **61**, 2933 (2016).
- ¹¹⁶T. Kishimoto and O. Nomoto, *J. Phys. Soc. Jpn.* **9**, 1021 (1954).
- ¹¹⁷S. V. Krivokhizha and I. L. Fabelinskii, *Sov. Phys.-JETP* **23**, 1 (1966).
- ¹¹⁸S. K. Kushare, D. H. Dagade, and K. J. Patil, *J. Chem. Thermodyn.* **40**, 78 (2008).
- ¹¹⁹S. V. Latha, G. Little Flower, K. Rayapa Reddy, C. V. Nageswara Rao, and A. Ratnakar, *J. Mol. Liq.* **209**, 153 (2015).
- ¹²⁰G. W. Marks, *J. Acoust. Soc. Am.* **41**, 103 (1967).
- ¹²¹A. K. Nain, *J. Mol. Liq.* **140**, 108 (2008).
- ¹²²R. Palani and A. Geetha, *Phys. Chem. Liq.* **47**, 542 (2009).
- ¹²³N. V. Sastry and M. C. Patel, *J. Chem. Eng. Data* **48**, 1019 (2003).
- ¹²⁴N. G. Tsierkezos and M. M. Palaiologou, *Phys. Chem. Liq.* **47**, 447 (2009).

- ¹²⁵M. Dzida, E. Zorębski, M. Zorębski, M. Żarska, M. Geppert-Rybczyńska, M. Chorążewski, and I. Cibulka, *Chem. Rev.* **117**, 3883 (2017).
- ¹²⁶C.-K. Li, A. N. Soriano, and M.-H. Li, *Thermochim. Acta* **487**, 26 (2009).
- ¹²⁷G. S. Parks and H. M. Huffman, *J. Phys. Chem.* **31**, 1842 (1927).
- ¹²⁸A. Pietrzak and K. Łudzik, *Fluid Phase Equilib.* **401**, 56 (2015).
- ¹²⁹J. A. Riddick, W. B. Bunger, and T. K. Sakano, "Techniques of chemistry," in *Physical Properties: Tabulations: Organic Solvents* (John Wiley & Sons, 1986), Chap. 3.
- ¹³⁰S. Herrig, M. Thol, A. H. Harvey, and E. W. Lemmon, *J. Phys. Chem. Ref. Data* **47**, 043102 (2018).
- ¹³¹R. Span and W. Wagner, *Int. J. Thermophys.* **18**, 1415 (1997).
- ¹³²M. Thol, G. Rutkai, A. Köster, R. Lustig, R. Span, and J. Vrabec, *J. Phys. Chem. Ref. Data* **45**, 023101 (2016).
- ¹³³R. Span and W. Wagner, *J. Phys. Chem. Ref. Data* **25**, 1509 (1996).
- ¹³⁴G. Venkatarathnam and L. R. Oellrich, *Fluid Phase Equilib.* **301**, 225 (2011).
- ¹³⁵R. Span, R. Beckmüller, S. Hielscher, A. Jäger, E. Mickoleit, T. Neumann, S. Pohl, B. Semrau, and M. Thol, TREND. Thermodynamic Reference and Engineering Data 5.0, Lehrstuhl für Thermodynamik, Ruhr-Universität Bochum, Bochum, Germany, 2020.
- ¹³⁶E. W. Lemmon, I. H. Bell, M. L. Huber, and M. O. McLinden, NIST Standard Reference Database 23: Reference Fluid Thermodynamic and Transport Properties-REFPROP, Version 10.0, National Institute of Standards and Technology, Gaithersburg, 2018.
- ¹³⁷I. H. Bell, J. Wronski, S. Quoilin, and V. Lemort, *Ind. Eng. Chem. Res.* **53**, 2498 (2014).